Next Generation Anodes for Lithium-Ion Batteries

Second Quarter Progress Report 2018

Dennis Dees, Point-of-Contact
Argonne National Laboratory
9700 South Cass Avenue
Argonne, IL 60439
Phone: (630) 252-7349
E-mail: dees@anl.gov

Brian Cunningham, DOE-EERE-VTO Technology Manager
U.S. Department of Energy, Battery R&D
Phone: (202) 287-5686
E-mail: brian.cunningham@ee.doe.gov

Table of Contents

Silicon Deep Dive Overview

Project Introduction

Silicon has received significant attention as a viable alternative to graphitic carbon as the negative electrode in lithium-ion batteries due to its high capacity and availability [1]. Elemental silicon can theoretically store >3500 mAh/g, nearly an order of magnitude higher than graphite (372 mAh/g and 818 mAh/mL, respectively). However, several problems have been identified that limit its utility including large crystallographic expansion (~320%) upon lithiation which translates to particle cracking, particle isolation, and electrode delamination issues. Further, there are fundamental and volume change related SEI stability issues, which affect cycling efficiency. The wealth of previous studies in this area is both a testament to its potential and the size of the challenge that must be overcome, requiring a great amount of innovation on multiple fronts.

BatPaC [2], a techno-economic program designed to model lithium-ion battery performance and cost, was utilized to establish program relevance by connecting DOE/USABC pack performance targets to anode targets. Generally, research with silicon containing anodes is focused on improving the specific capacity of graphite. However, this simple metric requires a more detailed analysis with factors such as the impact on average cell voltage, and volumetric capacity. It is notoriously difficult to select appropriate metrics that will enable an accurate calculation of the energy of a single electrode. Most methods estimate the volumetric energy density of active materials with the simplistic assumption that bulk density of the electrode does not undergo change in volume during cycling. While this serves well for most cathodes where the voltage can be fixed against lithium it is inappropriate for electrodes such as silicon.

As shown in Figure 1 (left frame), BatPaC calculations indicate anode volumetric capacities greater than 1000 mAh/cm^3 (= $\rho \cdot \varepsilon \cdot Q$ [g/cm$^3_{act}$ · cm$^3_{act}$/cm$^3_{elect}$ · mAh/g]) generally minimizes battery cost with an advanced NMC cathode. Note that higher capacities result in diminishing savings in cost. The analysis (right frame) also predicts that silicon-graphite electrodes with less than 75 wt% graphite can achieve the target. Finally, alloys of inactive metals (not shown) with silicon (or tin) can meet the volumetric capacity target as long as the metal choice is inexpensive (e.g. iron rather than nickel or cobalt).

Next Generation Anodes for Lithium-Ion Batteries, also referred to as the Silicon Deep Dive Program, is a five National Laboratory consortium assembled to tackle the barriers associated with development of an advanced lithium-ion negative electrode based upon silicon as the active material. This research program baselines promising silicon materials that can be developed or obtained in quantities sufficient for electrode preparation within the consortium facilities. Composite electrode and full cell development leverages recent investments made by DOE-EERE-VTO in electrode materials and characterization. The primary objective of this program is to understand and eliminate the barriers to implementation of a silicon based anode in lithium-ion cells. The Labs are focused on a single program with continuous interaction, clear protocols for analysis, and targets for developing both the understanding and cell chemistry associated with advance negative electrodes for lithium-ion cells. First and foremost, this undertaking is a full electrode/full cell chemistry project leveraging baseline electrodes prepared at the consortium facilities. All efforts are directed to understanding and developing the chemistry needed for advancing silicon-based anodes operating in full cells. Materials development efforts include active material development, binder synthesis, coatings, safety, and electrolyte additives. Efforts include diagnostic research from all partners, which span a wide range of electrochemical, chemical and structural characterization of the system across length- and time-scales. Specialized characterization techniques developed with DOE-EERE-VTO funding, include neutrons, NMR, optical, and X-ray techniques being employed to understand operation and failure mechanisms in silicon-based anodes. In addition, several strategies to mitigate lithium loss are being assessed. The project is managed as a single team effort spanning the Labs, with consensus decisions driving research directions and toward development of high-energy density lithium-ion batteries.

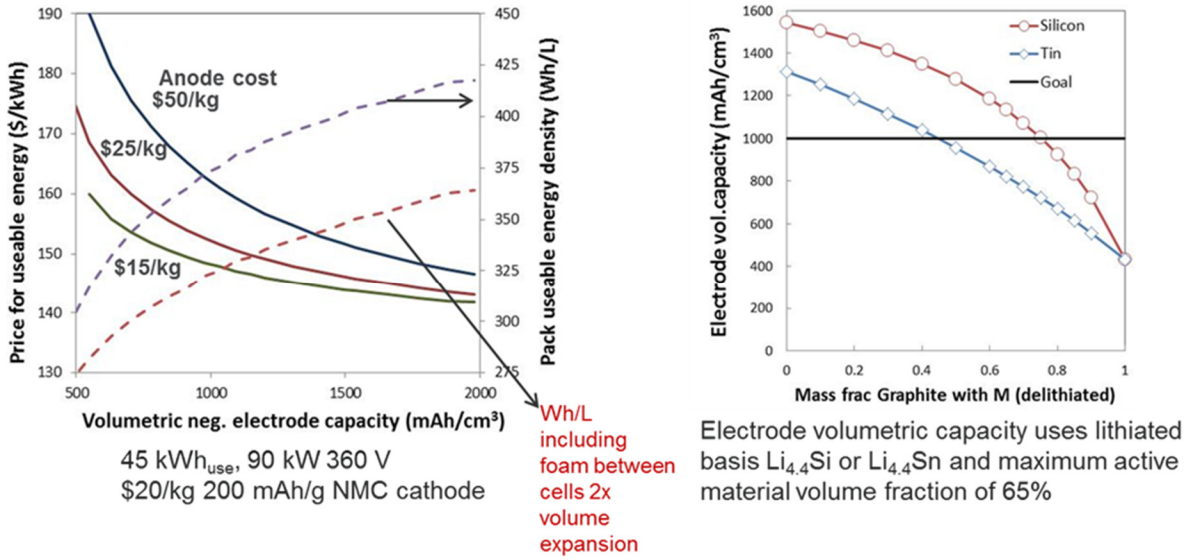

Figure 1. Battery Performance and Cost (BatPaC) model utilized to establish relevance by connecting pack to anode targets.

Objectives

- Understand and overcome the science and technology barriers to the use of silicon-based anodes in high-energy density lithium-ion batteries for transportation applications.
  - Stabilize the SEI
  - Stabilize the electrode
- Demonstrate functional prototype lithium-ion cell chemistries which meet the DOE/USABC performance targets.

Approach

Sandia National Laboratories (SNL), Oak Ridge National Laboratory (ORNL), National Renewable Energy laboratory (NREL), Pacific Northwest National laboratory (PNNL), Lawrence Berkeley National Laboratory (LBNL), and Argonne National Laboratory (ANL) have teamed together to form an integrated program. Technical targets have been developed and regular communications have been established. Throughout the program, there is a planned focus on understanding, insights into, and advancement of silicon-based materials, electrodes, and cells. All anode advancements will be verified based on life and performance of full cells. Toward that end, baseline silicon-based materials, electrodes, and cells have been adopted, along with full cell testing protocols.

In examining improvements, changes to the baseline cell technology will be minimized. As an example, silicon active material coating improvements will be verified on baseline silicon materials in electrodes fabricated by the battery research facilities. All other components in the prototype cells (i.e. positive electrode, separator, electrolyte …) will be from the baseline technology. There are many testing protocols that can be utilized to benchmark the baseline technology. This program has adopted a testing protocol from the literature [3] that has worked well for lithium-ion cells with silicon containing anodes. Shown pictorially in Figure 2 the test starts with three slow (C/20) formation cycles, an HPPC cycle, and then the C/3 aging cycles. The test ends with another HPPC cycle and three more slow (C/20) cycles. All constant current cycling is symmetric between charge and discharge rates. The tests are run at 30°C. If there is little or no aging in the first 100 cycles, the protocol can be repeated. This protocol effectively examines capacity, impedance, and aging effects in about a month's worth of testing.

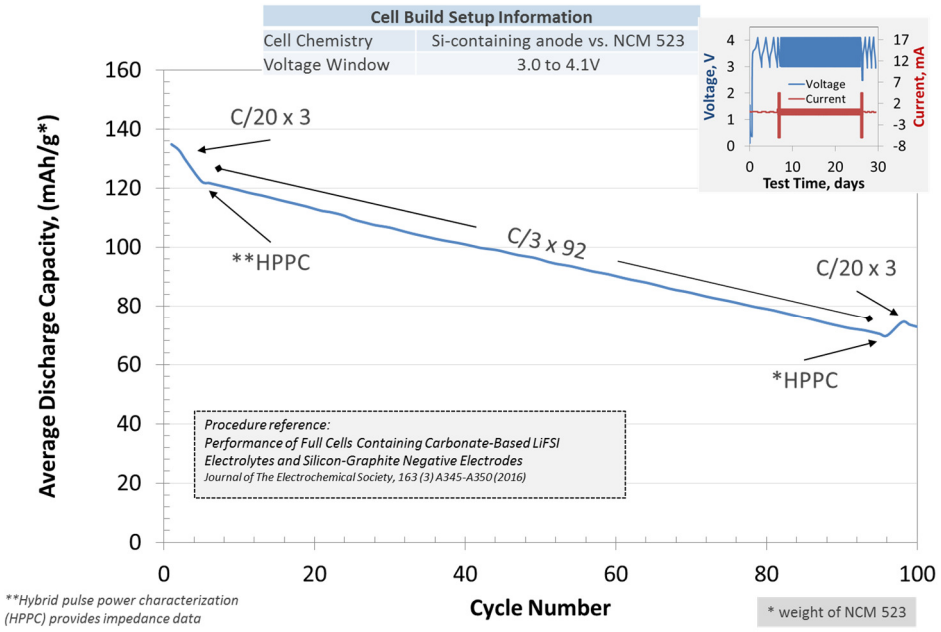

Figure 2. Full cell testing protocol.

As the program matures, materials developments will be incorporated into baseline silicon-based materials, electrodes, and cells. Scale-up of materials, incorporation of materials advancements into electrodes and prototype cells, and characterization and testing of cells, as well as evaluation of safety and abuse tolerance are part of a wide range of integrated studies supported by battery research facilities at the National Labs working closely with the program. These research facilities include the Battery Abuse Testing Laboratory (BATLab), the Battery Manufacturing Facility (BMF), the Cell Analysis, Modeling, and Prototyping (CAMP) facility, the Materials Engineering Research Facility (MERF), and the Post-Test Facility (PTF).

The fundamental understanding of silicon-based electrode active materials is based on extensive electrochemical and analytical diagnostic studies on components, electrodes, and cells conducted within the program. This effort contains in-situ and ex-situ studies on full and specialty cells, including reference electrode cells. Overall, the diagnostic studies are intended to help establish structure-composition-property relationships, including lithium-alloying surface and bulk transport and kinetic phenomena. Further, they should form the basis for accurately assessing component and electrode failure modes and lay a path for advancements.

Supported by the diagnostic studies, materials development on silicon-based materials, electrodes, and cells is being conducted to enhance interfacial stability, accommodate intermetallic volume changes, and improve overall performance and life. Key to this effort is the development and testing of coatings and additives designed to modify and stabilize the dynamic silicon-electrolyte interface. Further, functional polymer binders designed to accommodate volume changes, increase conductivity, and improve adherence are being developed and analyzed. Finally, the program is exploring active material development. Alternative high-energy silicon-alloy/composite materials are being considered. Also, strategies for introducing additional lithium inventory into the cell are being developed.

Communication of programmatic progress to battery community is critical. This will generally be accomplished through publications, presentations, reports, and reviews. Further, the program is open to industrial participation and/or collaboration that does not limit program innovation or the free flow of information. Finally, this program is highly integrated with our sister program on SEI-Stabilization, called SEI-Sta for short. In general, SEI-Sta is focused on the development and characterization of model systems, thin-film well-defined active area electrodes on which it is easier to extract fundamental information on lithium-silicon phase formation, lithium transport, and interfacial phenomena (e.g. SEI formation and growth).

References

1. *Alloy Negative Electrodes for Li-Ion Batteries*. M.N. Obrovac and V.L. Chevrier, Chem, Rev. 2014, 114, 11444-11503.
2. *Modeling the Performance and Cost of Lithium-Ion Batteries for Electric-Drive Vehicles*. Second Edition, Argonne National Laboratory Report, ANL-12/55.
3. *Performance of Full Cells Containing Carbonate-Based LiFSI Electrolytes and Silicon-Graphite Negative Electrodes.* S.E. Trask, K.Z. Pupek, J.A. Gilbert, M. Klett, B.J. Polzin, A.N. Jansen, and D.P. Abraham, Journal of The Electrochemical Society, 163 (3) A345-A350 (2016).

1. Research Facilities Support

CAMP Facility Support Activities

Steve Trask, Alison Dunlop, Andrew Jansen, Bryant Polzin (Argonne National Laboratory)

Background

The Cell Analysis, Modeling and Prototyping (CAMP) Facility at Argonne National Laboratory is providing support to this project in a number of different ways. The main contributions to the project are: providing standard materials, providing baseline electrodes (both anodes and cathodes) that are capacity matched, providing experimental electrodes as needed, and providing electrochemical data from coin cells and pouch cells that were tested by the CAMP Facility. By having access to these materials, (electrodes and data), other participating laboratories in the project are able to characterize and test the same materials using different techniques and test these materials in different configurations to make for a better comparison of data and are able to compare data across all laboratories working in this project. This provides a greater knowledge data pool for this project to draw from.

Results

In this Quarter, we worked on understanding the chemical makeup of the current and previously used silicon materials. We have had silicon material produced by several different methods: grown, ground and other novel methods. To possibly understand the processing differences and electrochemical performance differences, it is necessary to examine what impurities are present and what role they may play. To do this, we performed a full panel ICP-MS on various samples (see below).

The highlighted yellow rows show the main elements that show the differences between the silicon processing methods. The Ground samples show a similar impurity pattern. The main elements that show up are Ti, Zr, Y, and Hf. We can attribute these impurities to the grinding vessel and media used to produce the silicon powder. For the Nano Amor ground sample, the Na, Ca, Fe, and Ag content may be coming from the silicon feedstock that is used, but this not fully known. The Grown samples show two very different impurity profiles and probably indicates that two different methods were used to grow these particles.

From this data, we can conclude that the source of the silicon feedstock, along with the process used to make the silicon nano-particles plays a role in what impurities are present in the final product. As these materials are used, we will see if there is any correlation of impurity content to any processing results or electrochemical performance results.

	Paraclete Energy	Nano Amor	Nano Amor	Hydro Quebec	Paraclete Energy
CAMP Sample No.	F17-005-LS-AR	NA-70-130 APS	NA-50-70 APS	HQ-80 APS	4KD
	Ground	Ground	Grown	Grown	Ground
ACL Sample No.	18-0013-01	18-0017-01	18-0017-02	18-0027-01	18-0039-01
Li	< 1.08	2.51	1.58	< 0.79	< 0.47
B	< 4.04	5.31	< 1.53	5.87	NA
Na	12.6	244	247	< 0.78	0.8
Mg	< 0.37	6.73	10.2	28.8	< 1.64
Al	< 0.63	159	16.3	1040	< 2.04
Si	NA	NA	NA	NA	NA
P	< 12.4	20.5	< 8.21	< 15.9	< 19.2
K	< 10.9	< 6.82	< 7.22	23.2	< 5.0
Ca	< 25.8	122	26.4	172	< 10.5
Ti	101	1621	0.84	146	0
V	< 0.04	4.02	< 0.03	128	< 0.03
Cr	1.52	< 0.29	< 0.31	58.5	2.50
Mn	0.34	3.73	< 0.05	73.1	0.33
Fe	< 7.03	32.3	< 5.34	4427	< 13.26
Co	0.86	3.43	12.6	13.1	3.70
Ni	1.07	5.80	< 0.08	64.9	1.27
Cu	23.8	11.6	7.62	99.7	2.7
Zn	11.8	4.58	2.47	10.8	0.8
Ga	< 0.01	0.09	< 0.01	2.94	< 0.02
Ge	< 0.05	1.87	< 0.05	2.18	< 0.27
As	< 0.16	1.35	< 0.17	6.38	< 0.18
Se	< 1.33	< 0.87	< 0.92	< 2.54	< 3.29
Rb	< 0.01	< 0.01	< 0.01	0.10	< 0.01
Sr	< 0.02	0.31	< 0.08	1.13	< 0.07
Y	91.3	74.8	< 0.04	0.65	126.0
Zr	1428	1103	0.17	11.5	2001
Nb	< 0.03	0.30	< 0.01	0.95	< 0.18
Mo	< 0.15	1.00	< 0.17	5.43	< 0.40
Ru	< 0.01	< 0.02	< 0.01	< 0.01	< 0.01
Rh	< 0.01	< 0.02	< 0.01	< 0.01	< 0.01
Pd	< 0.02	< 0.02	< 0.02	< 0.22	< 0.02
Ag	< 3.90	65.5	< 0.02	3.86	< 0.27
Cd	0.76	0.77	< 0.03	< 0.04	0.70
Sn	< 0.04	0.35	0.08	0.92	< 0.16
Sb	< 0.02	0.25	< 0.04	0.88	< 0.05
Te	< 0.24	< 0.12	< 0.11	1.43	< 0.47
Cs	< 0.01	0.47	< 0.01	< 0.01	< 0.01
Ba	< 0.05	0.83	0.84	4.80	< 0.74
La	< 0.01	0.54	< 0.02	1.17	< 0.02
Ce	< 0.01	1.21	0.32	2.31	< 0.39
Pr	< 0.01	0.14	< 0.01	0.28	< 0.01
Nd	< 0.02	0.70	< 0.03	1.12	< 0.02
Sm	< 0.01	< 0.02	< 0.01	0.14	< 0.01
Eu	< 0.01	< 0.01	< 0.01	< 0.01	< 0.01
Gd	< 0.01	0.06	< 0.01	2.52	< 0.01
Tb	< 0.01	< 0.00	< 0.01	0.03	< 0.01
Dy	< 0.01	< 0.02	< 0.01	0.18	< 0.02
Ho	< 0.01	0.06	< 0.01	0.04	< 0.01
Er	< 0.01	0.03	< 0.01	0.08	< 0.02
Tm	< 0.01	< 0.01	< 0.01	< 0.01	< 0.01
Yb	< 0.01	< 0.01	< 0.01	0.05	< 0.01
Lu	< 0.01	< 0.01	< 0.01	< 0.01	< 0.02
Hf	50.2	39.3	< 0.01	0.34	50.9
Ta	< 0.01	0.17	< 0.01	0.20	< 0.76
W	< 3.53	< 3.73	< 1.35	< 1.66	< 1.32
Re	< 0.01	0.03	< 0.01	< 0.02	< 0.01
Ir	< 0.12	< 0.12	< 0.01	< 0.01	< 0.12
Pt	< 0.34	< 0.70	< 0.01	< 0.02	< 0.31
Au	< 0.06	< 0.14	< 0.05	< 0.06	< 0.09
Tl	< 0.01	< 0.01	< 0.01	< 0.01	< 0.06
Pb	0.62	1.86	0.76	1.53	0.16

Conclusions

As in past quarters, the CAMP Facility continues to provide the materials and data necessary to the project so that the overall project can move forward with consistent results. The CAMP Facility will continue to provide material support to this project in future quarters and will present new data as it becomes available.

Characterization and Optimization of Si Slurry by Zeta Potential

Kevin Hays, Beth Armstrong, and Gabriel Veith (Oak Ridge National Laboratory)

Background

One proposed strategy for the implantation of Si in Li ion batteries is the incorporation Si in graphite anodes. We have previously tested 15% Si – graphite composite anodes produced by large scale NMP slurry and aqueous slurry coatings, using a slot die roll-to-roll technique.[1] Both coatings displayed considerable particle aggregation of both the Si and carbon black particles in the graphite matrix. Inadequate particle surface charge in a high dielectric solvent result in a non-colloidal suspension, leading in poor dispersion and agglomeration of particles in the casted electrode. In order to address these issues, a more fundamental understanding of what is happening at the particle-solvent interface is necessary. Thus, we initially used phase analysis light scattering (PALS) to measure the zeta potential of various slurry components at several pH values.

Results

Individual slurry components were prepared in 1 mM KNO_3, in distilled water, by serial dilution. The salt is needed to attain the proper conductivity for PALS measurements. The zeta potential was measured at the native pH and subsequently titrated to other pH values using NH_4OH or HNO_3. Two different Si manufacturers (Nanoamor 70 – 130 nm Si and Paraclete F17-021-LS nSiO), carbon black (CB, Imerys C45), and graphite (Hitachi MagE3) were analyzed immediately after preparation and after 1 day (~24 hours) of equilibration. The role of the binder was also examined using Li substituted polyacrylic acid (LiPAA, LiOH titrated, Sigma Aldrich 1200 MW) at several pH values and concentrations.

Both Si particles investigated displayed a zeta potential very close to the isoelectric point (~ 3 to -20 mV) throughout most of the titration curve (Fig. 1A). This indicates a particle surface charge not greatly impacted by pH change. An exception to this is the Nanoamor Si, which differed from the Paraclete Si, such that at pH ~9.5 the zeta potential of the Nanoamor Si dropped rapidly to -34 mV, which is consider a stable colloid, where the Paraclete Si remained near -10 mV. Eventually, after 24h, the zeta potential of the Paraclete Si dropped to a similar zeta potential, at a pH ~ 9.5. This difference may arise from variation in the chemical composition at the surface of these particles. XPS (C1s) of the Paraclete Si, displayed a feature at 285.5 eV, not present in the spectrum from Nanoamor Si (Fig. 2A). This feature may result from an aliphatic solvent used in the grinding of the Si. The trend in zeta potential for both particles did not follow that of amorphous silica, which displays a much more negatively charged surface potential at high pH. Though these silicon particles have few nm SiO_x (1>x>2) shell, the assumption that these particle act like silica in water does not necessarily hold. In fact, these Si particles have a surface charge similar to that of CB and graphite through out most of the pH range, which could be linked back to the coverage of an organic species.

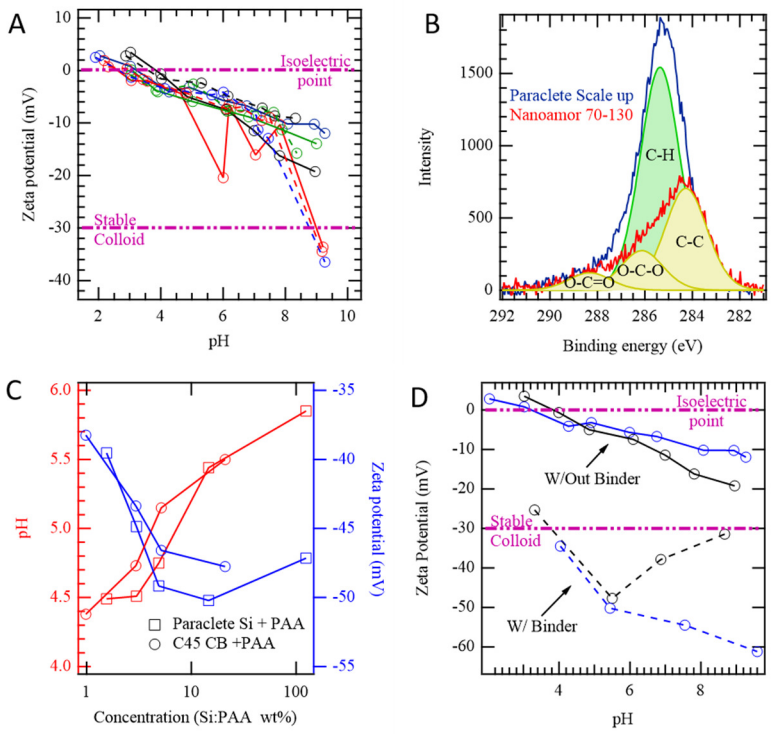

Figure 1 A) PALS measurement of Nanoamor Si (red trace), Paraclete Si (blue trace), CB (black trace), and graphite (green trace) directly after titration (solid line) and after 24 hours of equilibration (dashed line). B) XPS of C 1s orbitals of Nanoamor Si and Paraclete Si. C) Change of pH and zeta potential at various concentrations of Si to PAA, D) Change in zeta potential of Parclete Si and CB with and without PAA at optimized Si-to-PAA ratio, titrated with LiOH and HNO_3.

The binder's primary role is to provide particle cohesion and current collector adhesion, but it also can assist in slurry dispersion. Low molecular weight PAA was mixed with Paraclete Si and CB at various weight ratios (Fig. 1C). As the concentration of the PAA was decreased, the pH shifted from one dominated primarily by the PAA to that of the Si. At low concentrations, the PAA greatly improved the zeta potential, below -45 mV, of both the Si and the CB, with optimal concentration being ~15:1 (wt:wt) Si:PAA or CB:PAA. The addition of too much PAA decreased this effect, shifting the zeta potential above -40 mV (though still within the realm of a stable colloid). Using this optimized binder content, PALS measurements were completed on both Paraclete Si and CB over the full pH range. To replicate various levels of Li substation in LiPAA, LiOH was implemented in place of NH_4OH for the titrant. As the pH was increased in the Si/LiPAA dispersion, the zeta potential continued to shift more negative maxing out at -61 mV (pH ~ 9). Conversely, the CB reached a max of -50 mV (pH ~5.5) before decreasing at higher pH values.

Conclusions

PALS was used to analyze the zeta potential of slurry components in a Si-graphite composite anode. In an aqueous environment, the surface charge on all the particles are inherently unstable over a range of pH values. The lack of surface charge can lead to poor dispersion and particle agglomeration in the casted electrode. The incorporation of lower molecular weight LiPAA drove the zeta potential more negative for Si and CB, which likely will help improve the dispersion of these particles in the final slurry. Further optimization of graphite dispersion still must be completed, and other non-ionic dispersants may prove even better than the use of LiPAA alone. This data key in optimizing factors such as order of addition and slurry pH, and will assist in producing an optimized electrode formulation to minimize particle agglomeration.

References

1. Hays, K. A.; Ruther, R. E.; Kukay, A. J.; Cao, P.; Saito, T.; Wood, D. L.; Li, J., What makes lithium substituted polyacrylic acid a better binder than polyacrylic acid for silicon-graphite composite anodes? *Journal of Power Sources* **2018,** *384*, 136-144.

Thermodynamic Understanding and Abuse Performance

Kyle Fenton, Eric Allcorn, and Ganesan Nagasubramanian (Sandia National Laboratories)

Background

As we develop new materials to increase performance of lithium ion batteries for electric vehicles, the impact of potential safety and reliability issues become increasingly important. In addition to electrochemical performance increases (capacity, energy, cycle life, etc.), there are a variety of materials advancements that can be made to improve lithium-ion battery safety. Issues including energetic thermal runaway, electrolyte decomposition and flammability, anode SEI stability, and cell-level abuse tolerance behavior. Introduction of a next generation materials, such as silicon based anode, requires a full understanding of the abuse response and degradation mechanisms for these anodes. This work aims to understand the breakdown of these materials during abuse conditions in order to develop an inherently safe power source for our next generation electric vehicles.

The effect of materials level changes (electrolytes, additives, silicon particle size, silicon loading, etc.) to cell level abuse response and runaway reactions will be determined using several techniques. Experimentation will start with base material evaluations in coin cells and overall runaway energy will be evaluated using techniques such as differential scanning calorimetry (DSC), thermogravimetric analysis (TGA), and accelerating rate calorimetry (ARC). The goal is to understand the effect of materials parameters on the runaway reactions, which can then be correlated to the response seen on larger cells (18650). Experiments conducted showed that there was significant response from these electrodes. Efforts to minimize risk during testing were taken by development of a smaller capacity cylindrical design in order to quantify materials decision and how they manifest during abuse response.

Results

This work continues the efforts from last year, which aim to understand the fundamental reactions and quantify response from silicon based anodes under abusive conditions. This included evaluation of anodes containing between 0 and 15 wt% silicon from a variety of sources. Investigations were completed on coin cell and 1.25 Ah 18650 form factors. Several experiments showed a high level of gas generation and overall runaway for cells containing silicon electrodes. To further understand the response of these materials, this work focused on understanding the effect of several factors impacting runaway response and gas generation including solvent selection, electrode processing, silicon content, and the effect of water. Previous efforts to evaluate these parameters in 18650 cell form factors using

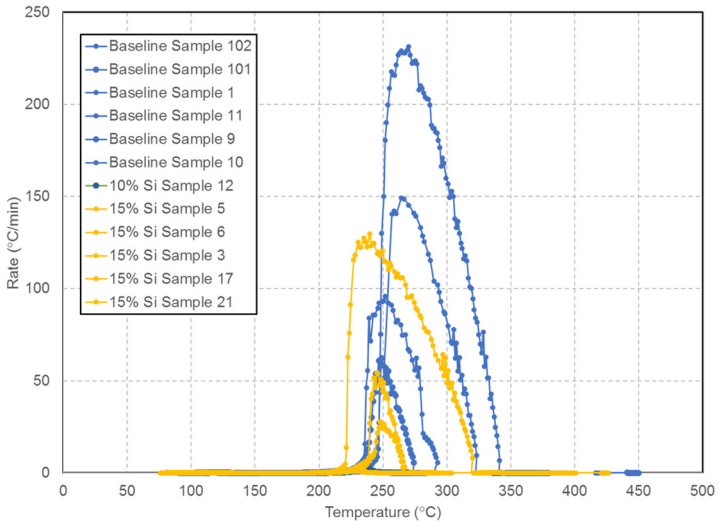

Figure 1 - Accelerating rate calorimetry (ARC) response for 18650 cells with graphite anodes (blue), 10 wt% silicon (green), and 15 wt% silicon (yellow). Heating rate is not normalized to active material content, so peak heating rates and overall runaway enthalpy is shown for qualitative purposes only.

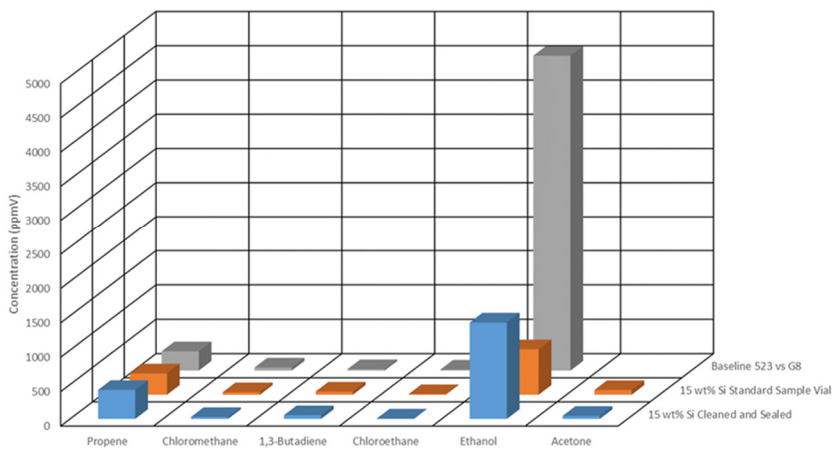

Figure 2 – Gas sampling analysis for hydrocarbons showing the differences of grab samples acquired during ARC evaluation in 18650 formats.

accelerating rate calorimetry (ARC) proved difficult due to the gas generation and temperatures involved during runaway. In order to try and quantify these effect, 18650 cells were made with electrodes cut to a much smaller overall cell capacity of roughly 600 mAh nominal capacity. The excess space within the cell was minimized using a copper insert to keep the ratio of electrolyte to electrode material constant. Figure 1 shows the ARC response for 18650 cells with graphite anodes (blue), 10 wt% silicon (green), and 15 wt% silicon (yellow). Heating rate is not normalized to active material content, so peak heating rates and overall runaway enthalpy is shown for qualitative purposes only. The overall response of the cells are very similar between graphite and silicon based composite electrodes. This result contradicts many of the observations seen in previous evaluation of silicon anode materials.

Figure 2 shows a subset of data from the analysis done on gas samples that were taken during ARC testing. This was done to try and evaluate species evolved during runaway. Gas analysis showed that the silicon containing electrodes generated higher levels of short chain hydrocarbons (ethane and propane), had less short chain organics (ethanol and propene), and similar concentrations of carbon dioxide and carbon monoxide. The overall gas generated in silicon based cells was about twice that generated in graphite containing cells.

Conclusions

This work demonstrates that there is an impact on safety response with nanoscale silicon materials compared to graphite based anodes. Changes to material and cell level properties can have impact on safety and thermal response characteristics. We have reported thermal runaway properties of cells (coin cells and cylindrical cells) containing nanoscale silicon up to 15 percent by weight. We continue to develop the understanding of abuse response for these anodes to better understand how these next generation negative electrode materials will impact cell and battery-level abuse tolerance. Additionally, the fundamental reactivity and gassing behavior that has been observed in silicon offers opportunities for better understand the safety of these materials.

Hydro/Solvothermal Synthesis and Scale-up of Silicon and Silicon-containing Nanoparticles

Youngho Shin, Gregory K Krumdick (Argonne National Laboratory)

Background

The immediate objective of this project is to develop and set up an advanced bench-scale hydro/solvothermal synthesis system for the production and evaluation of high-capacity engineered silicon nanoparticles and composites used as the active anode material in Li-ion batteries. These materials need to be tested and validated in large format prototype cells before going to high-volume manufacturing which use a fair amount of material. For this reason, the synthetic capability to be developed would be based on the design and construction of a turnkey hydro/solvothermal synthesis reactor system capable of batch production of 10 to 50 g of nanoparticles per run.

One of the features of the present process is to provide a bottom-up synthesis approach (stacking atoms onto each other) of silicon nanoparticles and composites which is more advantageous than the common top-down synthesis approach (etching out crystals planes) because the former has a better chance of producing nanostructures with less defects, more homogenous chemical composition, and better short- and long-range ordering. Using this advanced bottom-top synthesis approach, the crystallinity, particle shape and size of silicon nanoparticles incorporated into their composites, which are the key parameters of these materials' failure, should be intensely investigated and optimized to support the fundamental understanding of the EERE-VTO Energy Storage Si Deep Dive projects.

Results

The basic design for hydro/solvothermal synthesis system has been completed. The purchase procedure for long delivery and short delivery parts has been completed based on the basic design. The high-pressure and high-temperature reactor, which is the core equipment for the hydro/solvothermal synthesis system, was delivered as shown in Figure 1 below. We are now ready to install the system along with the other parts that are currently in stock.

Date	Description	Status
Oct-17	Project start	Done
Nov-17	System basic design	
Dec-18	Basic design review	
Jan-18	PO of equipment and parts	
Apr-18	System installation start	On track
May-18	WCD/ESH preparation	
Jul-18	Mechanical completion	
Jul-18	System safety review	
Aug-18	Revision and modification	
Aug-18	Operation permission	
Sep-18	Si nanoparticle synthesis	
Oct-18	30 g delivery to collaborator	
Nov-18	Si/C composite synthesis	
Dec-18	100 g delivery to collaborator	

Figure 1. Project milestones and arrived Hydro/solvothermal reactor

The mechanical completion of hydro/solvothermal synthesis system will be carried out in July. Safety related inspections will be conducted, and system improvements and corrections will be made on safety related issues. After completing all safety procedures, we plan to obtain an operation permit for the hydro/solvothermal synthesis system in August.

As we begin to synthesize silicon nanomaterials, we will first study synthetic process optimization related to particle size control of silicon nanomaterials. Silicon nanoparticle size and morphology will be controlled and optimized by adjusting operation pressure, temperature and reaction medium. This will be a guideline for synthesizing silicon nanomaterials of the desired particle size and distribution in the future. It is also a fundamental process research for the synthesis of complex compounds of silicon and carbon, or a combination of silicon and metal components.

Conclusions

We plan to synthesize silicon nanoparticles of various sizes after the set-up completion of the hydro/solvothermal synthesis system until September. After conducting a process study to control the particle size of silicon nanomaterials, we will synthesize a variety of silicon and carbon complexes by November. It is expected that silicon and carbon composite will uniformly distribute silicon and graphite in the laminate and improve the electrochemical performance of the anode.

2. Characterization, Diagnostics, and Analysis

Spectroscopic Characterization of Cycled Si Electrodes: Understanding the Role of Binder

Rose E. Ruther, Kevin Hays, Jagjit Nanda, and Gabriel Veith (Oak Ridge National Laboratory)

Background

The choice of polymer binder has a large impact on the cycling stability of Si-Gr composite anodes. Previously, we undertook a systematic study to separate several competing factors that influence the electrochemical performance of Si-Gr composites processed in water with lithium polyacrylate (LiPAA) binder compared to Si-Gr composites processed in NMP with polyacrylic acid (PAA) binder.[1] This study identified lower water content, higher coulombic efficiency, and lower impedance rise as the primary factors leading to better capacity retention with LiPAA-based anodes. Processing conditions may also influence cycling performance by changing the structure and uniformity of the electrode. To see if the different processing conditions impact the homogeneity of the composite, we used Raman micro-spectroscopy to map electrode composition and electrochemical reactivity for Si-Gr anodes processed using the two different formulations.

Results

Si-Gr composite anodes were cycled in full cells with NMC532 cathodes and standard electrolyte (90 wt.% Gen2 + 10 wt.% FEC). Cells were cycled between 3.0 and 4.1 V. Anodes were harvested from cells after 1 and 100 cycles, rinsed, dried, and analyzed by Raman spectroscopy without air exposure. To visualize anode heterogeneity, Raman maps were analyzed using basis analysis where each spectrum is treated as the linear combination of four components: c-Si, a-Si, carbon black, and graphite.

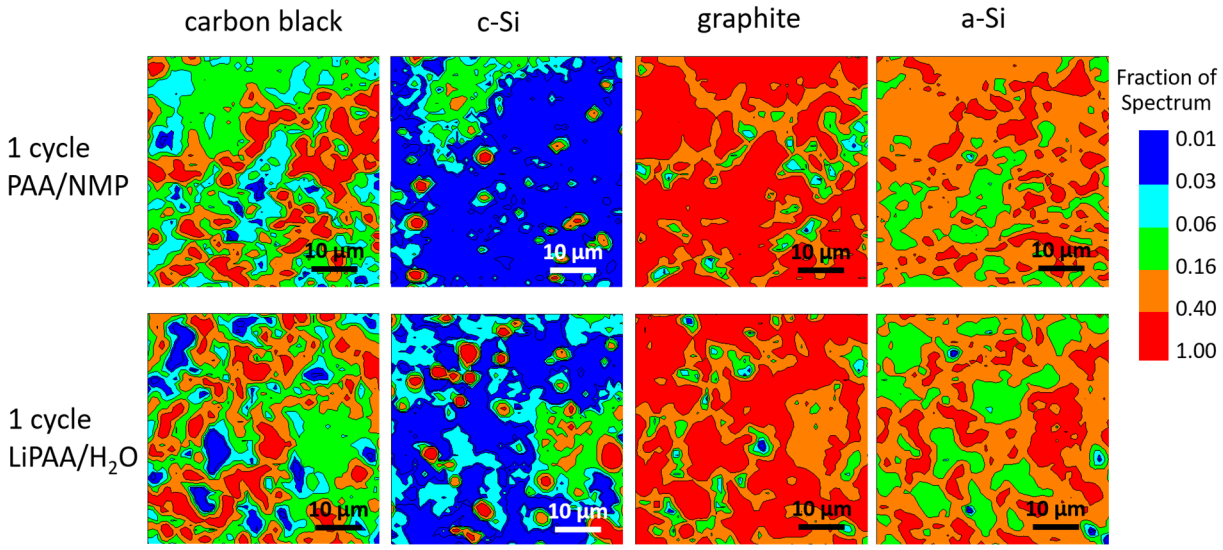

Figure 1. Raman maps of the distribution of carbon black, c-Si, graphite, and a-Si in Si-Gr composite anodes after 1 full cycle (lithiation and delithiation). The top row maps an anode made with PAA binder and the bottom row maps an anode made with LiPAA binder. Each map is 50 µm x 50 µm and comprises 2500 spectra. The color scale indicates the relative fraction of each component at each location across the map.

Processing the electrodes with PAA binder in NMP yielded a more uniform composite than water-based processing with LiPAA binder. The anodes processed from water showed more segregation of the silicon and graphite phases. In general, NMP-based processing resulted in better wetting and dispersion of silicon nanoparticles and carbon black in the slurry, which was reflected in the dried electrode. Despite differences in the quality of the pristine coatings, the first-cycle lithiation proceeded identically independent of the electrode binder (Figure 1). Both electrodes contained c-Si after one cycle, which indicates that some Si did not participate in the electrochemical reaction and convert to amorphous phases. Regions of electrochemically inactive Si were similar in size and extent in electrodes with PAA and LiPAA binder. Therefore, electrode uniformity and reactivity during the first cycle do not explain the improvements in long-term performance of the LiPAA-based anodes compared to the PAA-based anodes. Other factors such as residual moisture in the electrode appear to dominate.

References

1. Hays, K. A.; Ruther, R. E.; Kukay, A. J.; Cao, P.; Saito, T.; Wood, D. L.; Li, J., What makes lithium substituted polyacrylic acid a better binder than polyacrylic acid for silicon-graphite composite anodes? *J. Power Sources* **2018,** *384*, 136-144.

EQCM Studies of Silicon Anodes

J. Vaughey, Niya Sa, Binghong Han (Argonne National Laboratory)

Background

The DeepDive silicon program seeks to develop an understanding of the failure mechanisms of a silicon-based LIB anode and how the properties of a silicon-based electrode lead to those instabilities and short cell lifetimes. Many of the instabilities are thought to arise from the silicon particles SEI layer – its formulation, constituents, and dimensional stability – that acts as a buffer between the electrolyte and electrode surface. As the primary protective layer in a lithium-ion energy storage system, understanding the SEI layer is critical to

defining and understanding various failure mechanisms that lead to performance degradation as many of the causes of capacity fade and poor coulombic efficiency are, at their core, derived from an unstable SEI layer [1-4]. The reactivity of the surface of the silicon electrode is key to understanding the growth and stability of the SEI layer. In the DeepDive program we are focused on evaluating Si thin films during cycling to assess their reactivity with electrolytes using EQCM spectroscopy. This project addresses the stability of the electrode and the associated problems of the reactivity of the active material towards the constituents of the cell. This buildup of reaction products contributes to the fundamental problem of cycle to cycle instability associated with SEI layer.

Results

Efforts in the DeepDive program are focused on the synthesis and evaluation of thin film electrodes and their reactivity with the electrolyte. The main spectroscopic technique used has been electrochemical quartz crystal microbalance (EQCM). These surface based reactions are an important source of electrons and the formed organic reaction products that become substituents for the silicon SEI layer. In addition to our round robin effort, EQCM studies reported last quarter focused on studying the first cycle break-in process which noted that the mass of the deposited surface film increased in association with an increase in the porosity of the SEI layer. SEM studies confirmed film cracking (higher surface area) and delamination of the film from the EQCM sensor. These phenomena are consistent with the film delamination tied to the stresses induced on lithiation. In the past quarter we focused more on the role of FEC in the electrolyte. Comparing the CV curves of the thin film samples, addition of FEC causes the peak currents to shift towards OCV with 5% and 10% FEC addition, but further away from OCV with 20% FEC. The peak broadening seen for the 20% FEC samples indicates an increase of electrode resistance. This is consistent with the dilution of the electrolyte by

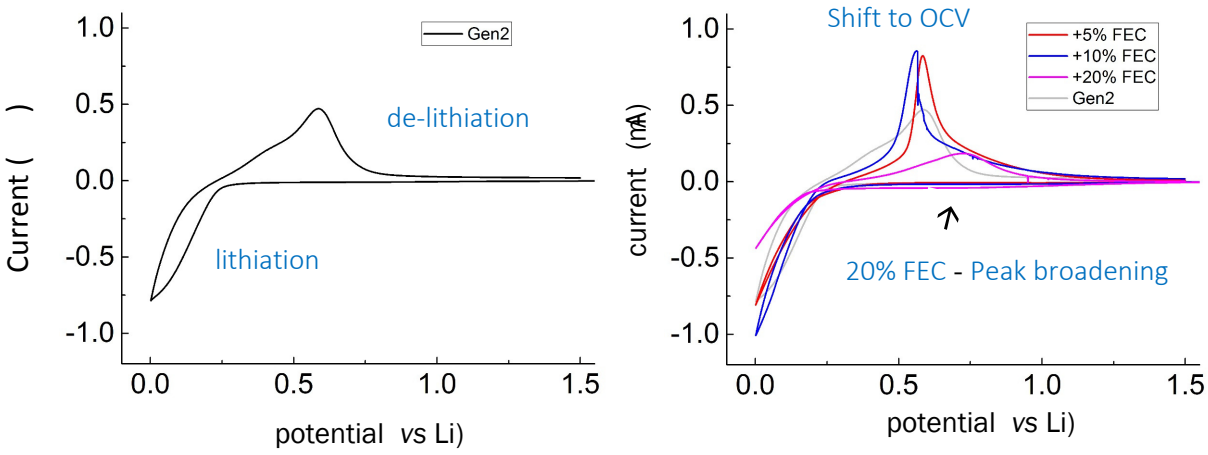

Figure 1. CV is scanned from the OCV (~2.8 V vs Li) to 0.001 V at 1 mV/sec. Comparison of the electrochemical response of a silicon thin film measured in Gen2 and Gen2+FEC electrolyte

FEC addition. As conductivity is an optimized variable, the dilution of the electrolyte by FEC reduces the overall salt molarity from 1.2M to ~1.0M effectively lowering the conductivity of the electrolyte. For the lower amounts of FEC addition to Gen2, the films produced at an FEC addition of 5% and 10% appears to facilitate Li diffusion in the bulk Si film, as well as the Li diffusion through the particle-electrolyte interface. Previous EQCM studies we reported on using these silicon films indicated that the main effect of adding FEC to the electrolyte was the significantly densify the SEI layer reducing porosity and increasing stability (minimal weight gain on cycling compared to the Gen2 baseline).

Conclusions

The SEI layer of silicon is a complex, every changing component of the lithium-based electrochemical cell. In our recent studies we noted the role of FEC in not only making a denser SEI film over the anode but that the film produced and electrochemical response of these films is tied to the method of FEC addition as it appears to act to dilute the electrolyte when at the 20% level effectively dropping the conductivity of the overall electrolyte.

Effect of silicate thickness on the electrochemical performance of silicate-coated silicon nanoparticles

Linghong Zhang, Kaushik Kalaga, Daniel Abraham, Wenquan Lu (Argonne National Laboratory)

Background

A Li_2SiO_3 coating has been reported beneficial for Li-ion batteries. When such a coating is present for a $LiNi_{0.6}Co_{0.}2Mn_{0.2}O_2$ cathode, improvement in both rate and cycle performance is observed owing to the excellent ionic conductivity of Li_2SiO_3 as well as the enhanced structural stability it provides[1]. A coating containing Li_2SiO_3 has also been applied to the Si anode. The resulting material showed improved capacity retention, however, with a compromised specific capacity.[2] Nonetheless, the improved capacity retention suggests that the Li_2SiO_3 coating may also improve the mechanical stability of the Si nanoparticles.

To further evaluate the effect of a silicate coating on the electrochemical performance of Si nanoparticles, Silicate-coated silicon nanoparticles with different thicknesses of silicates were synthesized via solid-state reaction. The particles were then characterized by XRD and tested for electrochemical performance.

Results

Figure1 shows the diagram for the synthesis of silicate-coated silicon nanoparticles. To obtain silicate-coated silicon nanoparticles of different silicate layer thicknesses, the Si nanoparticles with an average diameter of 80 nm were first treated at 400, 500, and 600℃ in the air for 15 hours to obtain a surface oxide layer of different thicknesses. The oxide layer thicknesses of the pristine Si sample and heat treated samples (from low to high temperature treatment) were estimated to 2.2, 2.8, 3.7, and 5.8 nm. The oxide layer thickness of the pristine Si is estimated to be 2.2 nm. All four Si nanoparticles were then mixed with Li_2CO_3 with a molar ratio of n(Si in SiO_2): n(Li in Li_2CO_3) = 1:2, and lithium silicate formation reaction was carried out at 800℃ under Ar atmosphere for 6 hours before collection for characterization.

Figure 1 Diagram for the synthesis of Li_2SiO_3-coated silicon nanoparticles

The silicate-coated Si nanoparticles were then characterized by x-ray diffraction performed at Advanced Photon Source at Argonne National Laboratory. The x-ray wavelength is 0.1173A. Figure 2 shows the x-ray diffraction patterns of silicate-coated Si nanoparticles with different initial oxide layer thicknesses of 2.2 nm, 2.8 nm, 3.7 nm and 5.8 nm, corresponding to pristine Si nanoparticles, Si nanoparticles treated at 400℃ in air, Si nanoparticles treated at 500℃ in air, and Si nanoparticles treated at 600℃ in air. The peaks corresponding to Si, Li_2SiO_3 and Li_4SiO_4 are labeled in the figure. A major formation of Li_2SiO_3 and a minor formation of Li_4SiO_4 are observed in all samples. As the thickness of the initial oxide layer increases, the peaks corresponding to silicates also increases in intensity, suggesting the formation of thicker silicate layers with thicker initial oxide layers.

The silicate-coated Si nanoparticles were then fabricated into laminates with 20 wt% LiPAA and 10 wt% C45. The electrodes were then tested in half-cell configuration with Gen II electrolyte (1.2 M $LiFP_6$ in EC: EMC=3:7) with 10 wt% FEC. The cells underwent three formation cycles at C/10 rate between 1.5 V and 0.01 V. Figure 3 shows the electrochemical performance of formation cycles for silicate-coated Si nanoparticles with different silicate layer thicknesses. As the initial oxide layer increases, the capacity obtained from the electrode decreases. Although a lower capacity (but better cycling stability) is expected for silicon nanoparticles with a thicker oxide layer, the capacity observed for all samples were lower than expected values. A likely cause of the compromised capacity is the formation of large aggregates from the solid-state reaction between Si nanoparticles and Li_2CO_3. The large aggregates of silicate-coated Si were observed under SEM. The presence of such aggregates likely leads to increased impedance in the electrode, causing the particles in the center of the aggregates not electrochemically active. Future work includes developing methods to break up the silicate-coated Si aggregates, as well as testing the electrochemical performance of the material.

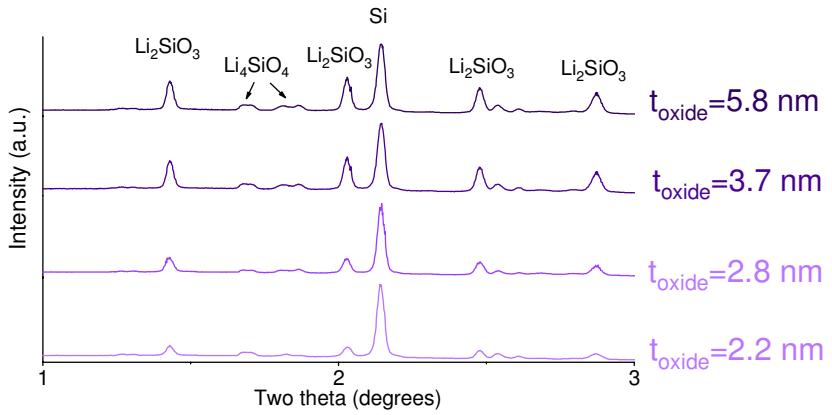

Figure 2 XRD patterns of silicate-coated Si with starting Si nanoparticles of different oxide layer thicknesses

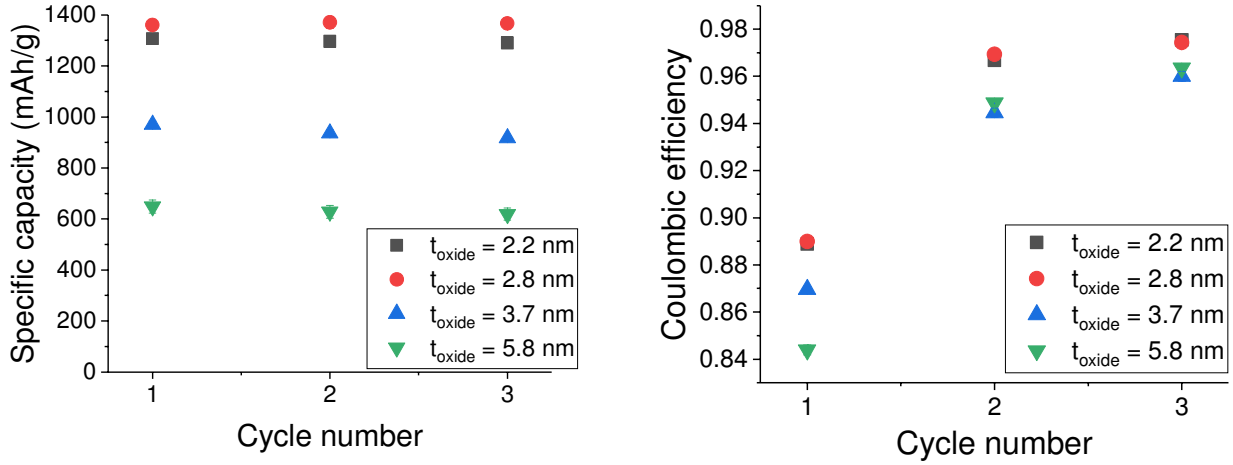

Figure 3 Electrochemical performance of formation cycles for silicate-coated Si with different silicate layer thicknesses

Conclusions

Silicate-coated Si consisting of major Li_2SiO_3 and minor Li_4SiO_4 were successfully synthesized via solid state reaction of the Si nanoparticles and Li_2CO_3. The silicate-coated Si showed compromised capacity in the initial electrochemical tests, with decreased capacity obtained with increased silicate layer thickness. A likely cause

of the low capacity is the presence of aggregates due to the solid-state reaction. Further study is undergoing to understand the phenomena and improve the capacity. Long-term cycling stability will then be tested.

References

1. Wang *et al*. "Enhanced the electrochemical performance of lithium metasilicate-coated LiNiCoMnO2 Ni-rich cathode for Li-ion batteries at high cutoff voltage", Electrochimica Acta, 2016, **222**, 806-819
2. Lee *et al*. "High-performance silicon-based multicomponent battery anodes produced via synergistic coupling of multifunctional coating layers," Energy Environ. Sci., 2015, **8**, 2075-2084

Calendar-life versus Cycle-life aging of Lithium-ion Cells with Silicon-Graphite Composite Electrodes – Electrolyte Analysis

K. Kalaga, S.E. Trask, I.A. Shkrob, D.P. Abraham (Argonne National Laboratory)

Background

The use of blended silicon-graphite (Si-Gr) negative electrodes increases the energy density of lithium-ion cells over those containing only graphite (Gr) electrodes. In a previous report we showed that the capacity loss of NMC532/Si-Gr cells is greater during cycle-life aging than during calendar-life aging. The repeated volume changes of the Si particles during cycling causes deterioration of the SEI layer, exposing surfaces, which are passivated by electrolyte reduction reactions that immobilize Li^+ ions. Volume changes are not expected in the Si particles during the potentiostatic hold step of the calendar-life aging tests. Yet, the cells showed some capacity loss (~3%) during this step indicating that the electrolyte reduction reactions continue (albeit slowly) on the lithiated Si particles.

In order to gain insights into the capacity loss mechanisms we examined the cell electrolytes after completion of the electrochemical tests. The electrolyte samples were collected into polypropylene containers, diluted 1:10 v/v with CD_3CN, and analyzed by nuclear magnetic resonance (NMR) using a Bruker Avance III HD (300 MHz). ^{19}F and ^{31}P NMR spectroscopy data were obtained on the electrolyte samples to track PF_6^- hydrolysis, as the products have different chemical shifts from the parent compound. For accurate integration of the ^{19}F and ^{31}P NMR resonances, 10-15 s delays were introduced between the excitation radiofrequency pulses. For comparison purposes we also conducted measurements on the fresh electrolytes, and on samples from as-prepared full cells that were held at open circuit for ~130 h after assembly *but never cycled*. These latter samples provided information on changes in the electrolyte during electrode "soaking", which was compared with changes to the electrolyte after formation cycling (~130 h is the time elapsed for three C/20 formation cycles).

Results

The electrolyte salt $LiPF_6$ is hydrolytically unstable. In solution, PF_6^- reversibly decomposes to F^- and PF_5 and the latter reacts with a water molecule to yield unstable POF_3 intermediate. Hydrolysis of POF_3 consumes another water molecule and yields the $PO_2F_2^-$ anion. All in all, this hydrolytic cycle converts a water molecule to two HF molecules. The greater is the PF_6^- conversion to $PO_2F_2^-$, the more HF is released. The moisture initially entering this cycle can be introduced from many sources. For our Si-Gr cells, the LiPAA binder is the primary source of water. The electrodes are fabricated using aqueous slurries that contain the binder; the polymers contain hydration-water that it is virtually impossible to remove fully during the thermal treatment of electrodes before cell fabrication.

Table-1 shows the mole fractions of the $PO_2F_2^-$ anion in the various electrolyte samples. No detectable $PO_2F_2^-$ was observed in the freshly prepared electrolytes. For the cell after three formation cycles, the mole fraction of $PO_2F_2^-$ anions in solution was low, ca. 2%. After cycle-life aging, this fraction increased to 6%. For the calendar-life aged cell (which was held at 4.1 V for 600 h) this $PO_2F_2^-$ fraction was considerably higher, ca.

25%. When the FEC electrolyte was simply put in contact with the electrode (no cycling) for 130 h (equivalent to time for formation cycles), the $PO_2F_2^-$ mole fraction was 11%. This value is considerably *higher* than the fraction in the cycle-life aged cells but *lower* than in the calendar-life aged cells. While this observation may appear paradoxical, reduced hydrolysis during cell cycling is expected because water is transformed into insoluble hydroxides when the negative electrode becomes lithiated. Without water in the electrolyte bulk, the $LiPF_6$ hydrolysis becomes arrested.

Table-1: Mole fractions of $PO_2F_2^-$ anion in electrolytes harvested from NMC532/Si-Gr cells with an electrolyte containing 10 wt% FEC in the EC:EMC (3:7 w/w) + 1.2M LiPF6 electrolyte

Cell	Mol% $PO_2F_2^-$
fresh electrolyte	≈ 0
Soaked for 130 h	11
After formation cycles	2
After calendar aging	25
After cycle aging	6

The data in Table-1 indicate that the extent of $LiPF_6$ hydrolysis in the electrolyte is ~ 4 times greater for *calendar*-life cells than for the *cycle*-life cells; that is, the chemical evolution of the electrolyte is different during calendar-life aging than during cycle-life aging. We propose the following explanation for the observations. When the Si-Gr cell is cycled and particle volumes change, the SEI becomes unstable, so HF can access and reacts with the surface. These reactions decrease the concentration of HF in the electrolyte. In contrast, during the potentiostatic hold, the SEI is not restructured so both water and HF can access the surface of the lithiated Si particles only slowly (by diffusion through the "static" SEI). Consequently, water has no reaction sink other than $LiPF_6$ hydrolysis; this is why the $LiPF_6$ hydrolysis becomes *so efficient*. However, even during the potential hold, some HF can reach the Li_xSi particle surface, where it corrodes the protective layer causing electrolyte reduction and the small (~3%) capacity fade mentioned above.

Conclusions

Electrolytes harvested from cells (with a NCM523-based positive electrode and a Si-Gr negative electrode) that were subjected to cycle-life or calendar-life aging were examined. Our data showed that the concentration of $LiPF_6$ hydrolysis products ($PO_2F_2^-$ anion, specifically) was significantly greater in the electrolyte from the *calendar*-life cells. Also, electrolytes that were simply in contact with the electrode (no cycling) showed significant amounts of the $PO_2F_2^-$ anion, indicating that the Si-Gr electrodes are a source of water in the cell (even though they are dried at 150°C in a vacuum oven). The HF generated during $LiPF_6$ hydrolysis can diffuse through the SEI and react with the Si particle surfaces. Such corrosion is more likely during cycle-life aging (which causes continuous restructuring of the SEI) than during calendar-life aging (wherein the SEI slows down, but does not prevent, HF access to the particle surfaces). Additional work is needed to identify coatings or electrolyte additives that protect the Si particles from the HF corrosion reactions.

3. Materials Advancements

Continued Study of Lithiation Effect of the Poly(Acrylic Acid) Binders on the Silicon Anode of Lithium-Ion Batteries

Bin Hu, Sisi Jiang, Zhengcheng Zhang, and Lu Zhang (Argonne National Laboratory)

Background

Lithiation of PAA binders is a common practice for silicon lithium-ion batteries, which could benefit the large scale lamination process by enhancing the shear thinning effect. It is also believed that the introduced lithium source could improve the cycling performance. However, lithiation processes involve strong basic lithium salt, LiOH, that dramatically impact the pH values of PAA polymers. Those changes may consequently lead to changes of the properties of PAA binders as they are pH-responsive. In addition, the surface of the Si particles tend to be more easily oxidized in basic environment, which led to generation of H_2. It is therefore of great importance that a better understanding of the role of PAA lithiation processes should be pursued and then an optimized lithiation condition should be suggested. In the last time's quarterly report, a chosen PAA binder with a molecular weight around 175k was carefully lithiated to different degrees via titration with LiOH solustions and the lithiation ratios were correlated to corresponding pH values. Those lithiated binders were then evaluated in half cells using Si/graphite (Si-Gr) composite electrodes. Such electrodes contain only ~15 wt% Si to reduce the overall expansion of the electrode during lithiation; both graphite and silicon serve as active materials in these composite electrodes. It is observed that less lithiated (or low pH) binders can lead to better cycling performance. FTIR results implies that less lithiated PAA binders may be more stable in the electrode matrix and cause less oxidation reactions of silicon particles. In this quarter report, we extended our efforts into full cell cycling and characterizations. While the least lithated binder continues to show great results, the one with pH = 6, surprisingly exhibits very comparable full cell cycling performance. Detailed characterizations have been conducted to seek plausible explanations.

Results

For the full cell evaluation, a CAMP supplied cathode, $LiNi_{0.5}Co_{0.2}Mn_{0.3}O_2$ (NCM523, C-015A), was used to couple with Si-Gr composite anodes, which was fabricated with the controllably lithiated PAA binders. **Table 1** shows the detailed information of PAA binders and Si-Gr electrodes. The full cells were then subjected to a standard testing protocol, which consisted of three formation cycles at a nominal C/20 rate, a hybrid pulse power characterization (HPPC) test, ninety-two aging cycles at a C/3 rate, another HPPC test and three final cycles at a C/20 rate, for a total of 100 cycles with the cell voltage between 3.0-4.2 V. The specific capacity profiles as well as the plot of area specific impedance (ASI) vs. cell voltage are shown in **Figure 1**. The processed cycling

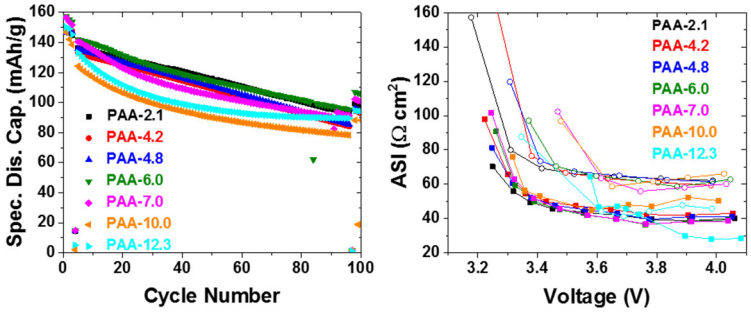

Figure 1. Specific discharge capacity profiles (to the left) for NCM523/Si-Gr full cells containing lithiated PAA binders with different pH values. Area specific impedance (ASI) vs. cell voltage (to the right) for NCM523/Si-Gr coin cells containing PAA binders with different lithiation percentage before (4th cycle, filled square) and after (97th cycle, open cycle) the C/3 cycles.

parameters, such as initial capacity, average capacity and capacity retention, are also summarized in **Table 1**.

Table-1: Information of the cell components, such as pH value of PAA binder, loading density of Si-Gr electrode, N/P ratio, as well as cycling parameters, such as initial specific capacity, average capacity and capacity retention results of the NCM523/Si-Gr full cells.

Cell	pH of PAA solutions	N/P ratio	Loading density (Si-Gr), mg/cm²	Initial specific capacity, mAh/g	Average capacity, mAh/g	Capacity retention, %
1	2.1	1.6	2.7	136.5	115.1	68.0
2	4.2	1.7	2.9	133.2	108.6	61.0
3	4.8	1.6	2.8	135.8	110.4	63.0
4	6.0	1.5	2.6	141.9	114.4	66.1
5	7.0	1.4	2.8	137.4	103.7	62.5
6	10.0	0.9	2.6	124.3	93.2	63.0
7	12.3	0.6	3.0	133.1	100.1	67.3

Unlike the cycling performance in half cells, which clearly indicated that increased lithiation can lead to more server capacity fading, the trend full cell results is less clear. As a matter of fact, except for **PAA-10.0** and **PAA-12.3**, whose N/P ratios are too low, all cycling results are comparable, implying the minimum effect of lithiaion of PAA binders. According to **Table 1**, the best performer is still **PAA-2.1,** a binder with no lithiation, and **PAA-6.0** nearly delivered the identical performance. The initial capacity, average capacity and capacity retention results of **cell 1-5** are within 10% range. Considering the variations of N/P ratios, it does seem that lithiating PAA may not impact the full cycling performance as much as in half cells. Similar results were also observed in ASI plot. Except for the low N/P value cells **PAA-10.0** and **PAA-12.3**, similar impedance values were observed for the rest cells before and after 92 cycles, while **PAA-2.1** indeed shows lower impedance at low voltage(~3.2-3.4 V). It is noted that the low N/P values of cell 6 and 7 are due to the significantly lower specific capacity resulting from the silicon reactions under basic conditions. One possible reason for those similar results are the relatively high N/P ratios, which may mask the performance difference of anode.

Figure 2 shows the Fourier-transform infrared spectroscopy (FTIR) of Si-Gr electrodes before cycling (left), after cycling in half cells (middle), and after cycling in full cells (right). We have compared the half-cell electrodes in the last quarter, which indicated a better presence of PAA in the less lithiated electrodes. Well, in the full cell cycled electrodes, some similar peaks are observed, such as Li_2SiO_3, Li_2CO_3, and PAAs. A new peak was observed at 1803 cm^{-1}, corresponding to the carbonyl groups in polycarbonates, which may imply SEI growth.

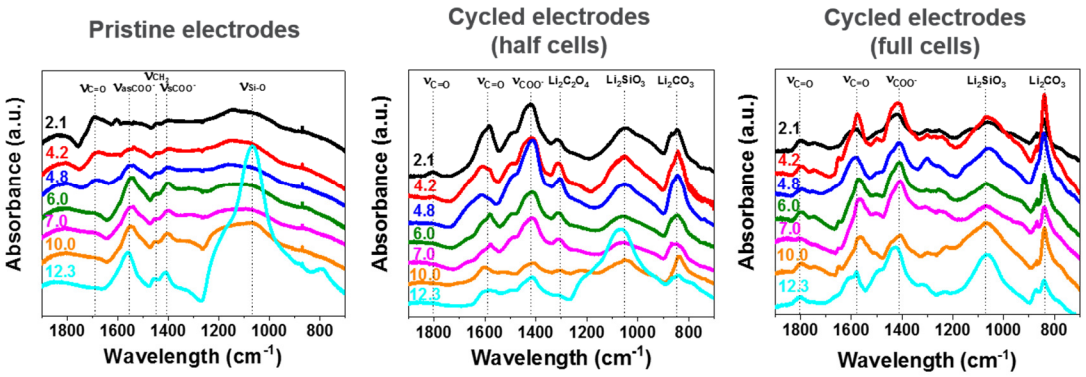

Figure 2. Fourier-transform infrared (FT-IR) spectra of Si-Gr electrodes before cycling (left), after cycling in half cells (middle), and after cycling in full cells (right).

Surface characterizations were also conducted to the cycled full cell Si-Gr electrodes. As shown in **Figure 3**, based on the scanning electron microscope (SEM) images, no obvious changes were observed from different cells. However, energy-dispersive X-ray spectroscopy (EDS) analysis indicates that O content increases as pH increases, which is consistent with our half-cell results. When the pH of the binder increases, the O content is increased from 20 % (PAA-2.1) to 27 % (PAA-10.0) and eventually to 57 % (PAA-12.3), which indicates significant oxidation of the silicon particles.

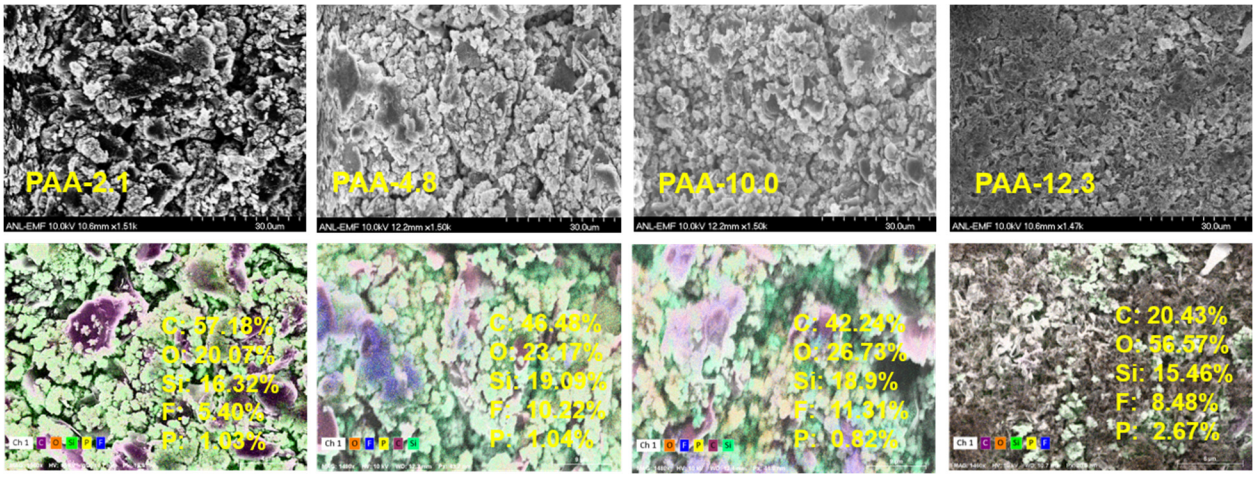

Figure 3. Scanning electron microscope (SEM) images and energy-dispersive X-ray spectroscopy (EDS) analysis of Si-Gr electrodes from cells **1, 3, 6, 7**.

Conclusions

In this quarter, we extend our effort of lithiation investigation of PAA binders to full cells. By comparing the cycling performance of full cells using controllably lithated PAA binders, it has been observed that regardless the lithation ratios, most cells delivered comparable cycling performance. One possible reason of the much less pronounced lithiation effect is due to the high N/P values of the full cells in this study. FTIR and SEM results once again confirmed that high lithiation or high pH PAA binders may lead to more serve silicon degradation. New cells with more reasonable N/P values will be tested.

Probe the relationships between functional electrolytes structure and SEI property for Si materials

Gao Liu, Tianyue Zheng (Lawrence Berkeley National Laboratory)

Background

Electrolyte decomposition products play a critical role in the stabilization of the negative electrodes in lithium-ion batteries, as the negative electrode is operated outside the stability window of the electrolyte. The electrolyte decomposition products form insoluble SEI layer, which stabilizes the electrode and electrolyte interface. Silicon alloy material has large volume expansion and surface reactions with the electrolyte when it is electrochemically lithiated. When delithiated, the Si alloy volume shrinks and surface area also decreases. This dynamic surface change causes excessive side reactions with the electrolyte. Moreover, some of the key electrolyte decomposition products are soluble in the electrolyte rather than solid precipitates. Surface coatings on Si materials by organic and ceramic have demonstrated improved surface stability towards electrolytes. Nano-sizing the Si materials can successfully prevent cracking of Si material. The Si particles are assembled by a functional polymeric binder to further improve the electrode stability in a composite electrode. We have demonstrated that both Si surface coating and functional binders can enhance cyclablity of the Si based composite electrode. Surface coating on Si can prevent electrolyte interaction with the reactive surface and

slow down the side reactions at the interface. Here, we propose to further reduce the Si surface reactivity by investigating electrolyte and additive functions to SEI formation and stabilization.

Results

This project is aimed to gain a comprehensive understanding of electrolyte decomposition products to SEI property relationship, and to guide the design and synthesis of new electrolytes and additives for Si based materials. New electrolyte design with consideration of the SEI structure and functions on the Si materials can lead to enhanced Si performance over the traditional mixed carbonate based electrolyte. Designing organic molecules with preferred decomposition pathways during electrochemical process can lead to controlled SEI formation on Si surface[4].

An effort to construct a bi-functional additive toolbox is underway (Figure 1). The bi-functional additive molecules have one reaction functional group to form coating on the surface of Si particles at low potentials, and another functional group to provide desired surface properties for the SEI layers. The reaction functional groups can also react with each other to form bulk polymer in a controlled organic chemistry environment. Figure 1d describe our previous work to synthesis bulk polyvinlyenecarbonate (PolyVC) polymer material. PolyVC can be used as binder and surface modifier for graphite based negative electrode to prevent propylene carbonate solvent molecules intercalation into the graphite layers.

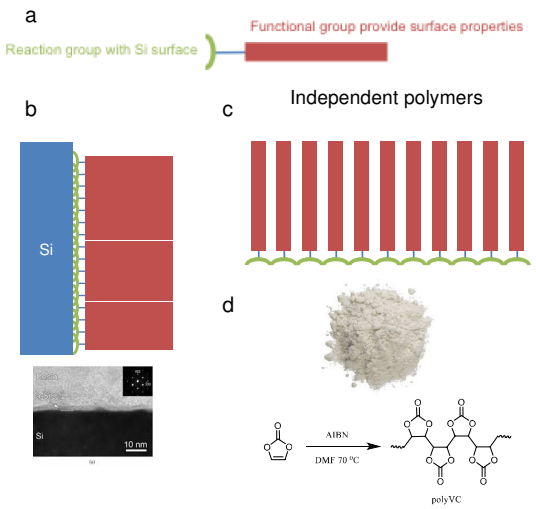

Figure 1. a. A schematic of bi-functional additives. b. Formation of surface layer on the Si surface. c. Formation of bulk polymer. d. An example of vinylenecarbonate polymerization to form polyvinylenecarbonate bulk polymer.

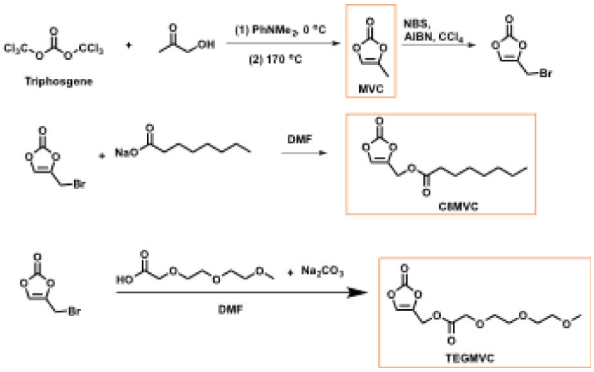

Figure 2. The scheme to synthesize the VC based bi-functional additives

The first group of bi-functional additives in the toolbox is based on a vinylenecarbonate reaction group and a hydrophilic or hydrophobic functional group (Figure 2). Three new additives are synthesized. The first one is MVC with an additive methyl group at the 3 position. The C8MVC has an extended hydrophobic alkyl group at the 3 position, whereas the TEGMVC has and extended hydrophilic ethyleneoxide group at the 3 position. The VC functional groups can react with the Si surface at low potential. The hydrophilic and hydrophobic chains can tune the properties of the Si surface layer. The synthetic scheme is developed and the intermediate and final products are qualified by the ^{1}H NMR spectroscopy.

An initial cyclic voltammetry tests (CV) are performed on the bifunctional additives (Figure 3). The base electrolyte is 1 M $LiPF_6$ in EC:EMC (3:7 by weight) solvent. The additive amount is 2% by weight. The CV tests are performed between 3V and 0.01V (Li/Li^{+}) potential range with Cu as working electrode and lithium

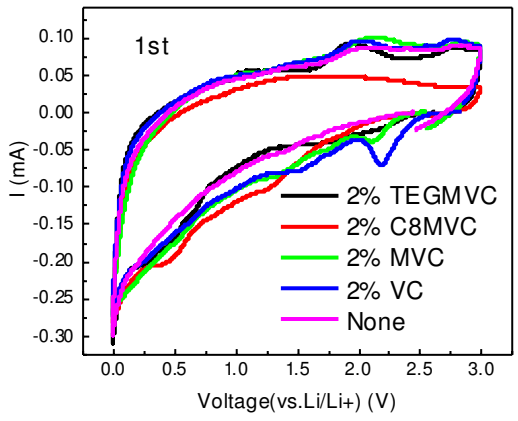

Figure 3. CV curves of the 2% additives in 1 M $LiPF_6$ in EC/EMC (3/7) base electrolytes.

metal as counter electrode. The scan rate is 10 mV/s. The base electrolyte is labeled as None as no additive inside of the electrolyte. The CV scans of base electrolyte against Cu working electrode shows no new peak in the first reduction wave from 2.5 V to 0.01 V. However, the CV scans of the electrolytes with additives show two groups of peaks in the first reduction scans. One group is from 1.0 to 2.5 V, and the other is around 0.5 V. The bifunctional additives decomposition on the Cu electrode is attributed to these reduction waves.

Conclusions

We have successfully designed and synthesized a group of bi-functional electrolyte additives with vinylenecarbonate as reaction group and a hydrophobic or hydrophilic chain as functional side groups. The initial CV tests are performed with this group of additives, showing different reduction waves compared to base electrolyte. Advanced electrochemical tests of the electrolyte additives to Si and graphite materials are underway to further characterize the additives. New reactive groups other than VC are also under investigation to develop a comprehensive structure for the bi-functional additive toolbox.

References

[1] M. Gu, X. C. Xiao, G. Liu, S. Thevuthasan, D. R. Baer, J. G. Zhang, J. Liu, N. D. Browning, C. M. Wang, *Sci Rep* **2014**, *4*, 7.

[2] F. F. Shi, P. N. Ross, H. Zhao, G. Liu, G. A. Somorjai, K. Komvopoulos, *JACS* **2015**, *137*, 3181-3184.

[3] S. J. Park, H. Zhao, G. Ai, C. Wang, X. Y. Song, N. Yuca, V. S. Battaglia, W. L. Yang, G. Liu, *JACS* **2015**, *137*, 2565-2571.

[4] H. Zhao, S. J. Park, F. F. Shi, Y. B. Fu, V. Battaglia, P. N. Ross, G. Liu, *JES* **2014**, *161*, A194-A200.

[6] H. Zhao, Y. Neslihan, G. Liu, et al. *JPS* **2014**, *263*, 288-295.

Silicon Surface Modification Using Molecular Layer Deposition

Taeho Yoon, Yanli Yin, Jasmine Meilissa Wallas, Chunmei Ban (National Renewable Energy Laboratory)

Background

The project aims to develop a systematic understanding and synthesis of surface coating materials to chemically or physically change the surface of the silicon (Si) materials, in order to improve the interphase chemistry, conductivity, and mechanical integration in Si-based electrodes. Continuous decomposition of electrolyte on the silicon surface is one of the factors dictating the electrochemical performances of Si electrode. Tremendous efforts have been dedicated in our lab to stabilizing the surface: (i) depositing an artificial protective layer (e.g., ALD or MLD), (ii) using a polymeric binder that mitigates electrolyte decomposition (e.g., PAA), and (iii) introducing electrolyte additives that sacrificially decompose to generate a protective film (e.g., FEC or VC). To study the fundamental roles of the surface species on the electrochemical and physical properties of the electrodes, we devoted FY 18 research to develop the liquid-phase deposition process to functionalize the silicon surface. The liquid-phase deposition are capable to explore various functional groups and can be applied for both laminated electrodes and the nanoparticles. The in-depth understanding from these studies will help establish effective mitigation to address the key challenges in Si-based electrodes; and develop strategies to deploy high-energy silicon alloys and composite electrode configurations in the full Li-ion cells.

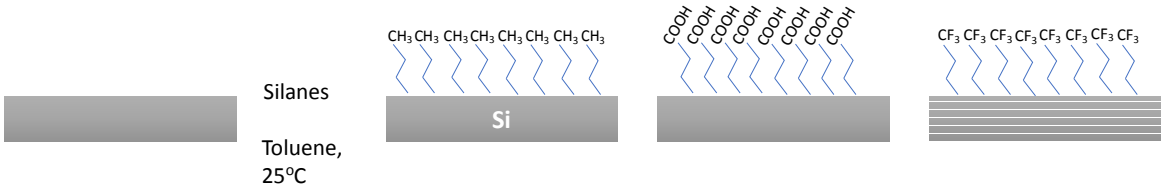

Figure 1. The illustration of electrodes prepared to investigate the effects of surface functional groups on SEI formation and its properties.

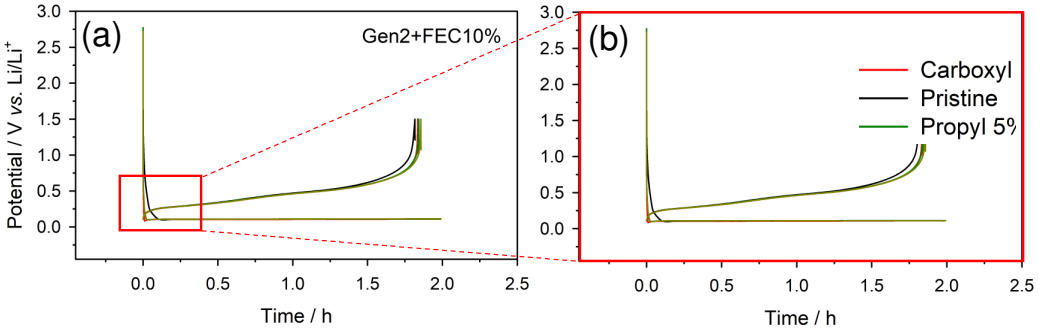

Figure 2. The voltage profiles of the functionalized electrodes. Cut-off : 2 hours lithiation, 1.5 V delithiation. Current density: 27.3 μA/cm^2.

groups show negligible impacts on the chemical composition determined by the XPS technique. That is, the SEIs on the treated surfaces are dominated by LiF as the SEI on the pristine electrode. Minor changes are observed in C, O, and Li spectra (not presented) especially on the surface of the CH_3-treated electrode, implying the different concentration of Li_2CO_3 or $Li_2C_2O_4$. Other spectroscopic measurements such as FTIR or TOF-SIMS will be performed to investigate the chemistry and structure of SEI on the functionalized Si electrodes.

Table 1. Chemical composition of SEI calaculated using XPS spectra.

Element	Pristine	-CH_3	-COOH	-CF_3
C 1s	8.8	13.9	10.5	11.2
Li 1s	35.8	34.1	35.6	35.3
F 1s	38.2	29.4	34.8	34.7
O 1s	9.6	15.7	12.9	12.3
P 2p	0.8	0.9	1.1	0.8
Si 2p	6.9	6.0	5.2	5.6

Electrochemical impedance spectroscopy (EIS) was used to evaluate the impact of the functional groups on the interfacial resistance of the Si electrodes. The EIS data were collected at the end of lithiation (1.5V) using 3-electrode cells. In the Nyquist plot in Fig. 3, the semi-circle in the high frequency region reflects the interface resistance; SEI (R_{SEI}) and charge transfer resistance (R_{ct}). The spike in the low frequency region is Warburg impedance of Li^+ diffusion in the electrochemical active material—Si electrode. Although the chemical compositions of the SEIs are comparable, the interface resistances are significantly different; the resistance increases in the order of -CH_3 (420 Ω) > Pristine (180 Ω) > -CF_3 (140 Ω) > -COOH (100 Ω). Assuming that R_{ct} is dominated by solvation and desolvation processes, the R_{ct} of each SEI should be similar because the chemistry of topmost SEI are comparable and the measurements were conducted with the same electrolyte. Thus, R_{SEI} is likely to be a main contributor to the interfacial resistance. Note that the state of lithiation would give a marginal effect on R_{ct} differences because the impedance of each electrode was measured at the end of lithiation. The deviation of the state of lithiation between electrodes is within 3 %. Further characterization is in process to elucidate the dominant factors of R_{SEI}.

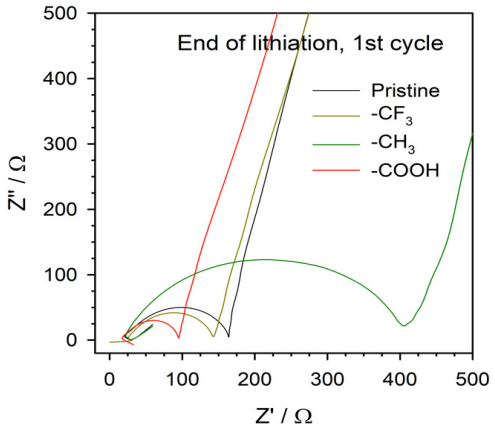

Figure 3. Impedances of the surface treated electrodes, measured at the end of lithiation

Conclusions

This integrated functionalization and chacterization approach allows exploring the role of the surface functional groups on SEI formation, electrochemical reversibility of Si electrode, lithium ion conductivity, and interfacial resistance.

The model silicon-wafer electrodes have been deposited with various silian groups of which the termination groups— -CH_3, -COOH, or -CF_3—have been used. The Coulombic efficiencies of the surface-coated electrodes are higher than that of the pristine electrode, in a order of -CF_3 (92.9%) > CH_3 (92.2%) > COOH (91.8%) > Pristine (90.9%). The interfacial resistance of all of the electrodes have been measured as -CH_3 (420 Ω) > Pristine (180 Ω) > -CF_3 (140 Ω) > -COOH (100 Ω). Although the SEIs on the treated Si wafers exhibit different behaviors in terms of ionic conductivity and electrochemical reversibility, the chemical compositions of the surfaces are comparable depending on the information from XPS analysis. To clarify the

disparity, further analysis of SEI composition and SEI thickness are in progress. Diverse functional groups would be explored to establish stronger understanding of the effect of functional groups. This work is expected to provide a fundamental insight for designing a binder, surface coating layer or electrolyte additives.

References

1. A. L. Michan, B. S. Parimalam, M. Leskes, R. N. Kerber, T. Yoon, C. P. Grey, and B. L. Lucht, *Chemistry of Materials,* **28** (22), 8149-8159 (2016)

Interfacial Modification of Si Anode for High Energy Li-ion Battery

John Zhang (Argonne National Laboratory)

Background

In this quarter, we continue to research the surface modification of silicon particles by electrochemical approach and organic synthesis approach. The former is to design new electrolyte/additive that could chemically/electrochemically decomposes and deposits on the lithiated Si surface forming a resilient SEI layer that stabilizes the interfacial reactivity of Li_xSi and electrolyte. Another approach is to functionalize the surface of Si particles through organic silane chemistry forming an artificial SEI for improved performance.

electrochemical performance of Si.

Results

1. Fluorinated Carbonates Electrolytes

In this quarter, new formulations of fluorinated carbonate electrolytes were investigated in Si-Graphite/Li half cell. They are 1.0 M $LiPF_6$ FEC/FEMC (5/5), 1.0 M $LiPF_6$ DFEC/HFDEC (5/5), 1.0 M $LiPF_6$ TFPC/FEC/FEMC (1/1/1) and 1.0 M $LiPF_6$ TFPC/DFEC/HFDEC (1/1/1). **Figure 1a** shows the capacity retention and Coulombic efficiency of the Si-Graphite/Li cells with different fluorinated electrolytes. After a fast capacity decay in the initial cycles, the FEC/HFDEC cell was stabilized with the highest capacity and capacity retention, whereas the TFPC/DFEC/HFDEC cell was the worst performing cell (blue profile). The low specific capacity is due to the high current used (C/2) for these tests. The lithium salt impact on the Si anode was also studied in this quarter. LiFSI was chosen as a new lithium salt and its impact when combined with fluorinated electrolytes was summarized in **Figure 1b**. New electrolyte with 1.0 M LiFSI dissolved in FEC/FEMC (5/5) outperformed other fluorinated electrolytes and the baseline electrolyte 1.2M $LiPF_6$ EC/EMC (3/7 in weight) plus 10% FEC (the red profile in Figure 1b).

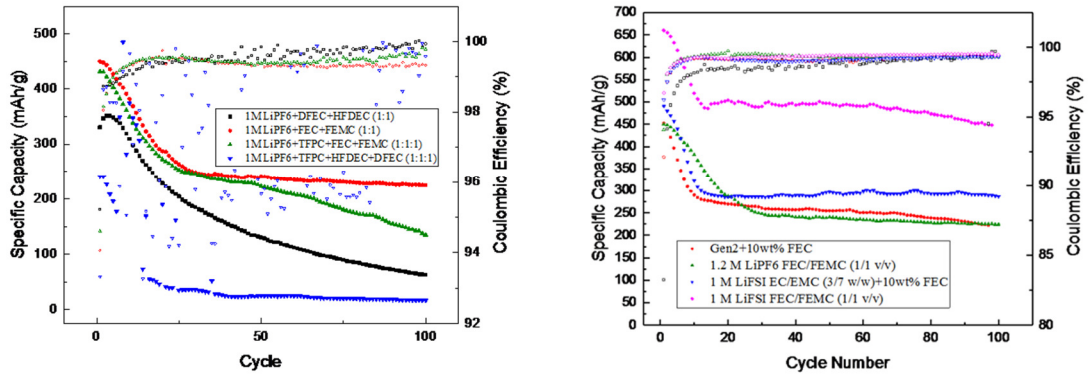

Figure 1. (a) Capacity retention and Coulombic efficiency of Si-graphite/Li cells with fluorinated electrolyte 1.0 M $LiPF_6$ FEC/FEMC (5/5), 1.0 M $LiPF_6$ DFEC/HFDEC (5/5), 1.0 M $LiPF_6$ TFPC/FEC/FEMC (1/1/1) and 1.0 M $LiPF_6$ TFPC/DFEC/HFDEC (1/1/1); (b) Capacity retention and Coulombic efficiency of Si-graphite/Li cells with fluorinated electrolyte using LiFSI as salt. (C/2 for charge and discharge, the cutoff voltage is 0.01-1.5 V).

2. Si Particle Surface Functionalization

Last quarter, we have synthesized Si nanoparticles (Si-O-Epoxy NPs) with glycidoxypropyl trimethoxysilane (GPTMS). Its improved battery performance leads us to explore more epoxy-functionalized Si particles. Figure 2 showed the chemical structure of the different epoxy silanes used for Si particle surface modification.

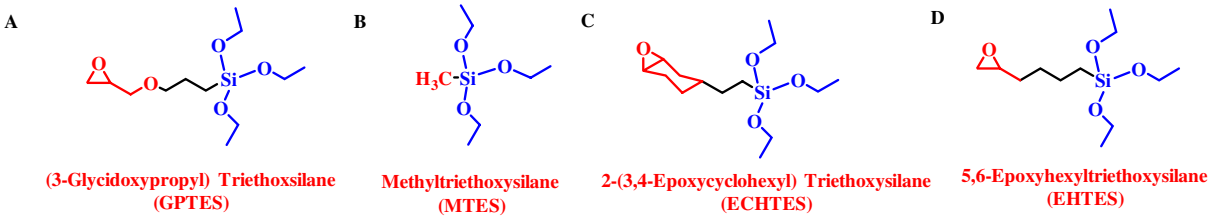

Figure 2. Chemical structure of new epoxy containing silanes used for Si particle surface modification.

Si nanoparticles Si-Epoxy NP and Si-Cylcoepoxy NPS were synthesized using 5,6-epoxyhexyltriethoxysilane (EHTES) and 2-(3,4-epoxycyclohexyl) triethoxysilane (ECHTES) and their TGA profiles were shown in **Figure 3a**. The Si-Cycloepoxy PS decomposed rapidly when the temperature reached 500 °C, and lost 4.0% at 800 °C, whereas Si-O-Epoxy NPs gradually lost weight with increasing temperature. The weight loss indicates the successful attachment of the epoxy groups onto the silicon particle surface.

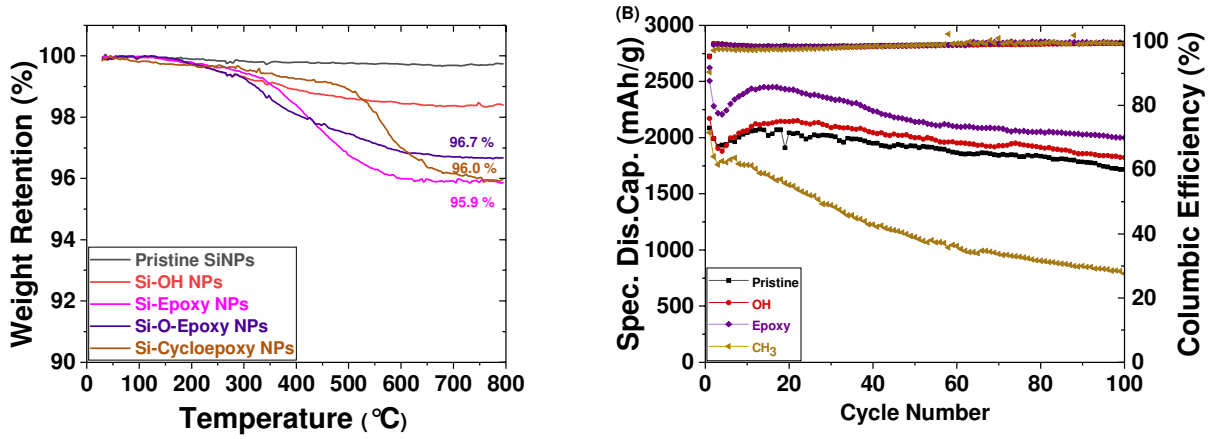

Figure 3. (a) TGA profiles of pristine Si NPs, Si-OH NPs, Si-Epoxy NPs, Si-O-Epoxy NPs and Si-Cycloepoxy NPs; and (b) capacity retention and coulmobic efficiency of Si/Li half cells with pristine Si NPs, Si-OH NPs, Si-O-Epoxy NPs and Si-CH_3 NPs.

The anode electrode was prepared with 70% surface functionalized Si-NH_2 and Si-Epoxy particles, 10% Timcal C45 and 20% PAA aqueous solution, which was then evaluated with 2032 coin cells. Charge-discharge cycling was performed between 0.01-1.5 V with a current rate of C/3 following three formation cycles at C/20. **Figure 3b** showed the cycling performance of the Si-O-Epoxy NP/Li cell. Si-O-Epoxy NPs outperformed the pristine Si particle and the Si-OH NP in terms of initial capacity and the cyclability. This is the first surface functionalized Si NP sample that demonstrated its effectiveness in promoting its electrochemical performance. This result is encouraging and motivates us for extensive future screening research.

Development of High Energy Metals

Wei Tong (Lawrence Berkeley National Laboratory)

Background

Fluoroethylene carbonate (FEC) is an effective electrolyte additive for Si-based anodes. Most studies focus on understanding of its role at a low concentration (≤ 30 wt%) rather than completely replacing the conventional solvent, ethylene carbonate (EC). In this quarter, we studied the functionality of FEC and its impact on Si electrode surface morphology and composition by comparing EC- and FEC-based electrolytes, specifically, 1M $LiPF_6$ in EC-diethyl carbonate (DEC) and 1M $LiPF_6$ in FEC-DEC (50: 50 wt%). Binder-free freestanding Si-multi-walled carbon nanotube (Si-MWCNT) composite electrodes were used for this study.

Results

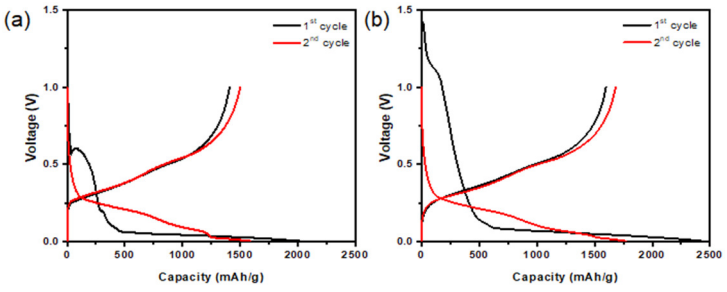

Figure 1. The 1st and 2nd cycle voltage profiles of Si-MWCNT electrodes with (a) EC-DEC and (b) FEC-DEC electrolytes.

Si-MWCNT composite electrodes, with Si to MWCNT mass ratio of 3:2 and a thickness of ~ 40 μm, were assembled using Li metal foil as a counter electrode. The areal mass loading is ~ 3 mg/cm^2. The cells containing EC-DEC or FEC-DEC electrolytes were cycled in a voltage range of 1 - 0.005 V *vs.* Li/Li^+ at a current of 280 mA/g. Specific capacity is based on the total mass of Si-MWCNT electrodes. The 1st and 2nd cycle voltage profiles are presented in Figure 1.

The initial slopes during the 1st lithiation process are attributed to electrolyte decomposition and solid-electrolyte interphase (SEI) formation. The 1st lithiation/delithiation capacity of 2025 and 1409 mAh/g and coulombic efficiency (CE) of 70% were achieved with EC-DEC electrolyte vs. 2429 and 1598 mAh/g and 66% for FEC-DEC electrolyte, respectively. As shown in Figure 1b, FEC-based electrolyte decomposition occurs at a higher potential (> 1 V) than conventional EC-based electrolyte. Both slopes related to SEI formation disappeared in the subsequent cycle.

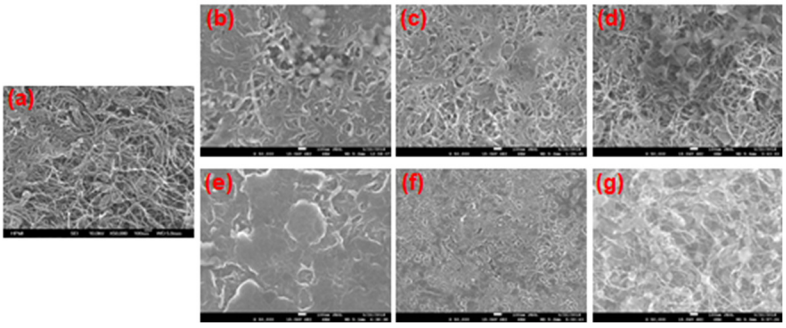

Figure 2. SEM images of Si-MWCNT electrode at (a) pristine, (b, e) 1st lithiation, (c, f) 1st delithiation, (d, g) 2nd delithiation states, where (b-d) EC-DEC and (e-g) FEC-DEC electrolyte.

The morphology of pristine and cycled electrodes with different electrolytes was examined by scanning electron microscopy (SEM). CNT and Si nanoparticle features were clearly observed on the surface of pristine electrode (Figure 2a), and a deposited layer formed on the surface of electrodes after the 1st lithiation in both electrolytes (Figure 2b, e), particularly, CNT features were almost invisible when cycled in FEC-based electrolyte (Figure 2e). After the 1st delithiation (Figure 2c, f), reduced SEI coverage on the surface was observed, suggesting the possible SEI decomposition and/or dissolution. Interestingly, the morphology of the cycled electrodes after the 2nd delithiation (Figure 2d, g), where the distinct features of Si and CNTs were visible, resembled more pristine electrode rather than that after the 1st delithiation. This maybe an indication of the chemical/electrochemical instability of surface species. Table-1 shows elemental distribution in cycled Si-MWCNT electrodes. All elements are normalized to Si for comparison. In general, O-containing species decreased upon delithiation and increased upon lithiation on the surface of electrodes cycled in both electrolytes, which seems consistent with the surface morphology change observed by SEM. Additionally, more F-containing compound was present in FEC-based electrolyte.

Table-1: Elemental distribution in Si-MWCNT electrodes cycled in EC-DEC and FEC-DEC electrolytes. Elements are normalized to Si (at%).

Eelectrolyte	Cycled State	C	O	F	P
EC-DEC	1st Lithiation	3.7	6.3	0.9	0.02
	1st Delithiation	3.0	2.3	0.3	0.01
	2nd Lithiation	4.6	7.9	0.4	0.01
	2nd Deithiation	3.2	2.2	0.4	0.02
FEC-DEC	1st Lithiation	2.5	4.2	0.9	0.02
	1st Delithiation	5.8	1.9	1.1	0.02
	2nd Lithiation	3.9	5.9	1.7	0.02
	2nd Deithiation	3.5	2.2	1.5	0.04

Conclusions

Surface film morphology and composition of Si-based electrodes cycled in EC- and FEC-based electrolytes were studied. A deposit layer of clearly different surface morphology was observed in EC-, FEC-based electrolytes after the 1st lithiation, however, such morphology was disappearing in the subsequent cycle in both electrolytes. These results suggested the possible difference in chemical/electrochemical stability of SEI components in different electrolytes. In next quarter, we will prepare amorphous Si and Si-Sn thin film electrodes and continue the studies of SEI components in different electrolytes.

Si anodes with extended cycle life and calendar life

Ji-Guang Zhang, Xiaolin Li (Pacific Northwest National Laboratory)

Background

Nano Si or highly porous structured Si has been widely used to avoid pulverization of Si particles during cycling process. However, large surface area of nano Si or micron sized porous Si may also lead to a continuous reaction between lithiated Si and electrolyte. As a result, this reaction may lead to continuous growth of SEI layer and increase of cell impedance. Another possible degradation mechanism is the cross talk between Si anode and cathode. The mitigation of dissolved Mn in cathode may poison Si anode; FEC additive which is highly effective in forming a stable SEI layer on Si may form a detrimental cathode electrolyte interface (CEI) on cathode surface which also leads to impedance increase. Therefore, minimize the surface area of Si and find a stable electrolyte additive are critical for long term stability of Si based Li-ion batteries.

In this project, we will enhance the cycle life and calendar life of Si based Li-ion batteries by designing a stable porous Si structure and develop an artificial SEI layer coated on the surface of porous Si particles. A more stable electrolyte additive or solvent mixture will be developed to minimize the detrimental effect of FEC currently used in Si based Li-ion batteries. The degradation mechanism of Si anodes during shelf storage will be systematically investigated. New insight on these mechanisms and the new approaches developed in this work will speed up the deployment of high energy Li-ion battery with Si-based anodes and increase market penetration of EVs and PHEVs as required by DOE/EERE.

Results

In last quarter, we showed the excellent long-term cycling performance of hierarchical Si-Carbon nanotube microsphere (HSCM) anodes in both half-cell and full-cell configurations. In this quarter, the swelling and mechanical property of the HSCM anodes are further studied to understand the correlation of structure and electrochemical performance. In situ TEM characterization was carried out to observe the particle volume expansion during lithiation process. Figure 1a-c showed TEM images of the Si/MWNT particles taken at different lithiation stage. The primary Si nanoparticles fully lithiated to from amorphous alloy (inset of Figure 1c), but the apparent volume expansion of the secondary spheres is only ~34.5% indicating the hierarchical structure developed in this work is effective in mitigating the swelling and pulverization of Si materials. The electrode is expected to have limited swelling and hence good mechanical and electrical integrity during cycling.

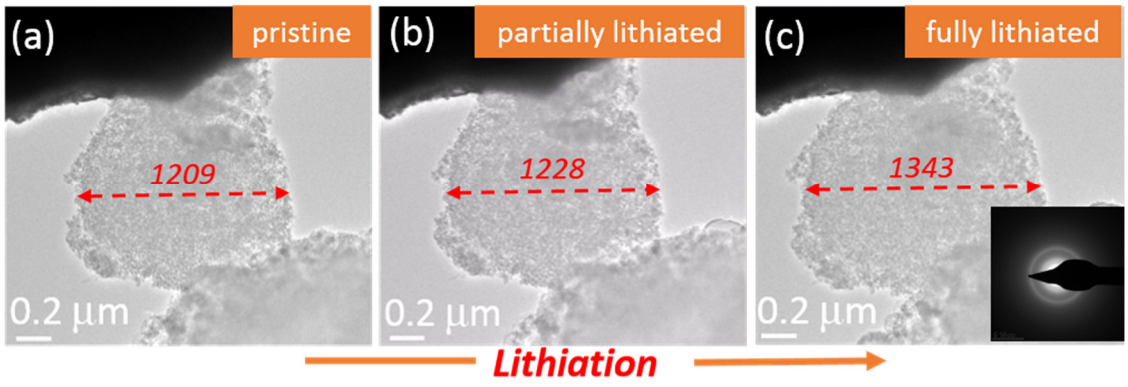

Figure 1. In situ TEM characterization of the lithiation process of a typical Si/MWNT microsphere. a) Si/MWNT composite particle before lithiation; b) partially lithiated particle; c, fully lithiated particle. Inset is SAED pattern of a lithiated sphere, showing its amorphous character. The unit for the data in the Figures is “nm”.

The Si/MWNT also showed very good mechanical strength. Figure 2 showed the in-situ SEM and AFM measurement of the compressing of a typical Si/MWNT microsphere of ~8 micron. The pressure for the AFM tip to start penetrate the microsphere is ~220 MPa. The designed structure has very good mechanical strength and is expected to have intact structure under calendering.

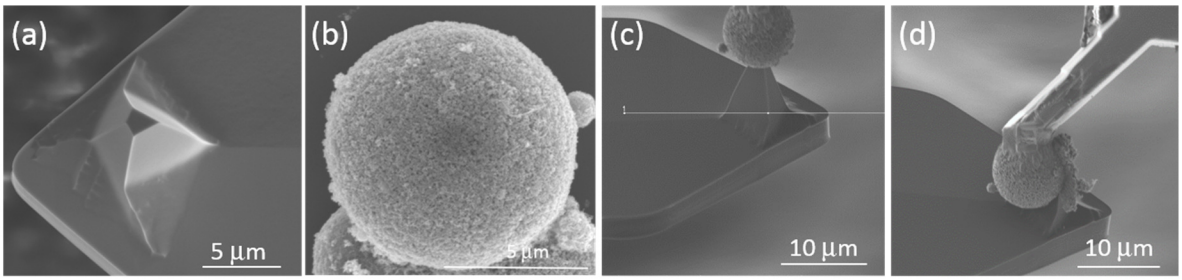

Figure 2. In-situ SEM-AFM indentation of a HSCM particle. a) SEM image of the AFM Tip; b) high resolution SEM image of the particle before the compressing; c) SEM image of the contact between AFM tip and the particle before the introduction of the force; d) SEM image of the particle broken after the introduction of a large force.

Conclusions

The unique structure of HSCM delivers the promised effect on minimizing the apparent swelling of Si upon lithiation and delithiation and maintain the structural integrity. And the unique design of Si/MWNT also shows excellent mechanical robustness.

References

1. Hierarchical-structured, silicon-based electrodes and methods of making same, Haiping Jia, Ji-Guang Zhang, and Xiaolin Li, U.S. patent filed on Nov. 2017.

Lithium Inventory

C. S. Johnson and W. M. Dose (Argonne National Laboratory)

Background

Lithium inventory excess is required in order to enable Si-containing anodes in high energy advanced Li-ion batteries. The question arises: what is Li inventory, and how does it function in a cell? First off, we classify Li inventory in three schemes. First is the reversible cyclable Li, second, the Li that is consumed on the first cycle (first cycle irreversible capacity loss), and (for Si, maybe) the next few formation cycles thereafter. And third, the Li consumed cycle to cycle in long-term cycles. The second feature is typically negotiated via a burst of Li in the first cycle either from a Li additive (such as Li_5FeO_4 or LFO pre-lithiation additive in the cathode), or from pre-lithiating Si-graphite composites electrochemically formed prior to cell build.

For graphite anodes, the passive film SEI produced naturally from reduction of EC-containing ester carbonate solutions protects the electrode from further Li-consumption reactions. Since the first cycle irreversible capacity loss is minimal in the graphite anode system, one can easily match the n/p electrode capacity ratio, and the cyclable Li is reasonably accountable. However, as has been demonstrated in multiple studies, Si (de)alloying reactions and the associated large volume changes cycle to cycle causes fresh surfaces to be exposed to the electrolyte, thus requiring new passivation (and Li consumption) processes essentially siphoning off cyclable Li. Therefore, in addition to a large first cycle irreversible loss, the per cycle cumulative losses makes it quite hard to determine what initial n/p ratio to use. Thus one objective from Li inventory is to suggest the correct n/p ratios. We continue to work on this deep understanding of cumulative

cycle-to-cycle capacity losses for the Si-anodes in full cells. Herein, we report on pre-lithiation of 5 V spinel, $Li_{1+x}Ni_{0.5}Mn_{1.5}O_4$ as a potential means to add Li inventory into the Si-graphite cell.

Results

We have been addressing Li inventory on three fronts previously and these are bulleted below.

- First approach is to use a full cell (instead of Li half cell), whereby a ***high-capacity $LiFePO_4$ pseudo-reference/counter electrode is utilized***. This allows us a diagnostic tool to track capacity losses without complication of Li metal survivability in the cell over 1000 cycles.
- ***Introducing Li inventory to the cell #1***. We have continued to investigate ***Li_5FeO_4 as a pre-lithiating source*** for the Si-containing anode. We still have to establish the cyclability of a blended LFO- NMC cathode and understand any cross-reactivity, impedance changes, capacity changes in the resultant electrode, and this is the focus moving forward in the next quarter.
- ***Introducing Li inventory to the cell #2.*** Last quarter we presented ***over-lithiated NMC, or $Li_{1+x}NMC532O_2$*** as a potential way to feed Li to the Si anode from Li release on the first charge via the cathode. It seems that the % weight increase (<2%) where x=1 is minimal could be advantageous, and, at the same time would allow the introduction of Li with subsequent NMC532 active phase used. However, in quarter 1, the result of over-lithiated NMC532 in a Li half cell showed that the material's electrochemical performance is adversely affected by over-lithiation, probably as the result of irreversible anisotropic c-axis enlargement and associated volume increase.

Another way to introduce Li into the Si-containing cell, is via a lithiated 5 V spinel, or $Li_{1+x}Ni_{0.5}Mn_{1.5}O_4$. In this context, the 5 V spinel could serve the role of having active capacity in the NMC532 layered cell as an additive, but also be electrochemically active under a certain optimized voltage window. Nevertheless, to test the ability of lithiated 5 V spinel to first work in a Si-graphite cell, we chemically lithiated the 5 V spinel with Li(ammonia) reaction, isolating a product with composition $Li_{1.62}Ni_{0.5}Mn_{1.5}O_4$. This lithiated oxide was stable in air, and could be laminated outside. Once made, it was paired with a Si-graphite electrode as anode. The cycling performance is shown in Figure 1.

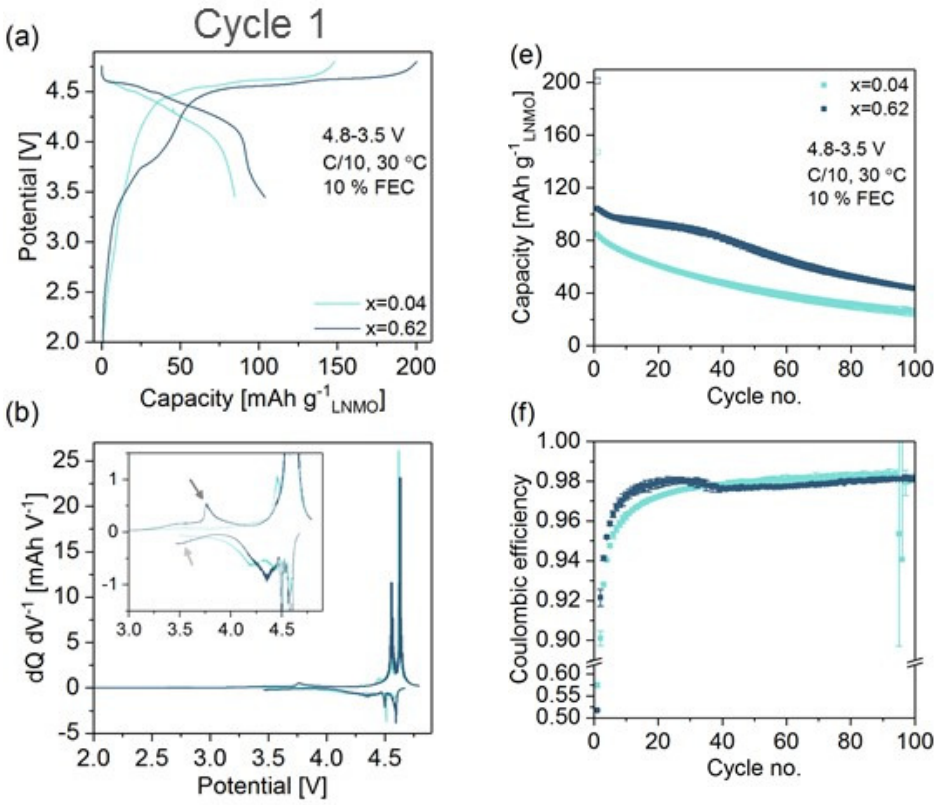

Figure 1. (left, a. b.) Si-graphite/$Li_{1+x}Ni_{0.5}Mn_{1.5}O_4$ cell first cycle voltage profile (top), and (bottom) the corresponding dQ/dV curve, and (right, e., f.), the capacity versus cycle number plot (top, e.) and coulombic efficiency plot (bottom, f.). Conditions of cycling are indicated in the Figure. **Note the darker blue curves are with x=0.62 (lithiated), and light blue with x=0.04 (non-lithiated baseline).**

These results indicate that the pre-lithiated 5 V spinel with x=0.62 can act to improve the capacity observed over that of the control cell. Future experiments will feature blended 5 V spinel and NMC532 layered electrodes tested versus Si-graphite anodes.

Conclusions

A lithiated 5 V spinel was chemically synthesized with $Li_{1.62}Ni_{0.5}Mn_{1.5}O_4$ composition. The additional 0.62 Li can be used as Li inventory in a Si-graphite containing full cell on the initial cycle. To this end, we observe that the pre-lithiation into the cell helps the capacity utilization. About 71% higher capacity is seen after 100 cycles. Capacity retention can be improved by providing lithium inventory to mitigate the 1st cycle irreversible capacity loss. In this way, it is likely that the Si is cycling in a more reversible electrochemical window and less electrode voltage slippage is occurring. To test this hypotheses, we plan to work with the diagnostic team with three-electrode cells in the Si deep dive project.

References

Published paper

W. M. Dose, M. J. Piernas-Munoz, V. A. Maroni, S. E. Trask, I. Bloom, and C. S. Johnson, Capacity fade in high energy silicon-graphite electrodes for lithium-ion batteries, *Chemical Communications*, 2018, **54**, 3586 – 3589 & inside back cover art.